Article

Cell Reports

The RNA-Binding Protein Rasputin/G3BP Enhances the Stability and Translation of Its Target mRNAs

Graphical Abstract

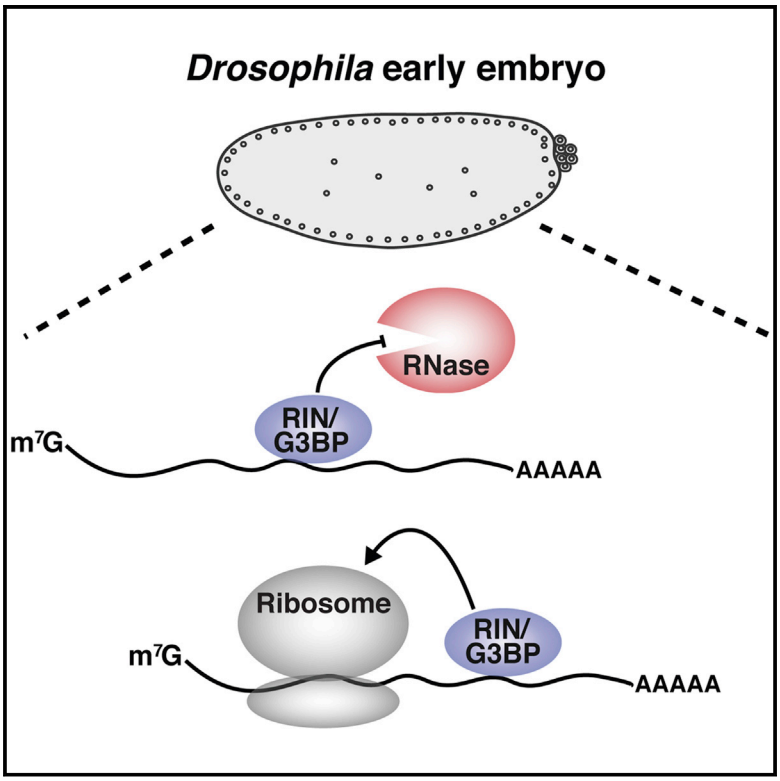

Authors

John D. Laver, Jimmy Ly, Allison K. Winn, ..., Stephane Angers, Craig A. Smibert, Howard D. Lipshitz

Correspondence

c.smibert@utoronto.ca (C.A.S.), howard.lipshitz@utoronto.ca (H.D.L.)

In Brief

Laver et al. show that in early embryos, Rasputin, the *Drosophila* G3BP ortholog, binds short mRNAs and is associated with polysomes. They provide evidence for a direct role for Rasputin and its human homologs in stabilizing and upregulating the translation of their target mRNAs.

Highlights

- In early embryos, the *Drosophila* G3BP Rasputin (RIN) is polysome associated
- RIN binds over 550 mRNAs, which are short, stable, and highly translated
- In rin mutants, steady-state levels of its target mRNAs are reduced
- Tethering RIN or human G3BPs enhances the expression of a luciferase reporter mRNA

Laver et al., 2020, Cell Reports *30*, 3353–3367
March 10, 2020
https://doi.org/10.1016/j.celrep.2020.02.066

CellPress

Cell Reports
Article

The RNA-Binding Protein Rasputin/G3BP Enhances the Stability and Translation of Its Target mRNAs

John D. Laver,[1,7] Jimmy Ly,[1,2,8] Allison K. Winn,[2] Angelo Karaiskakis,[1] Sichun Lin,[3] Kun Nie,[1] Giulia Benic,[1] Nima Jaberi-Lashkari,[1,2,8] Wen Xi Cao,[1] Alireza Khademi,[1] J. Timothy Westwood,[4] Sachdev S. Sidhu,[1,5] Quaid Morris,[1,5,6] Stephane Angers,[2,3] Craig A. Smibert,[1,2,*] and Howard D. Lipshitz[1,9,*]

[1]Department of Molecular Genetics, University of Toronto, 661 University Avenue, Toronto, ON M5G 1M1, Canada
[2]Department of Biochemistry, University of Toronto, 661 University Avenue, Toronto, ON M5G 1M1, Canada
[3]Department of Pharmaceutical Sciences, University of Toronto, 144 College Street, Toronto, ON M5S 3M2, Canada
[4]Department of Biology, University of Toronto, 3359 Mississauga, Mississauga, ON L5L 1C6, Canada
[5]Donnelly Centre, University of Toronto, 160 College Street, Toronto, ON M5S 3E1, Canada
[6]Vector Institute, 661 University Ave, Toronto, Ontario, Canada, M160 College Street, Toronto, ON M5G 1M1, Canada
[7]Present address: Department of Cell and Systems Biology, University of Toronto, 25 Harbord Street, Toronto, ON M5S 3G5, Canada
[8]Present address: Department of Biology, Massachusetts Institute of Technology, Cambridge, MA 02139, USA
[9]Lead Contact
*Correspondence: c.smibert@utoronto.ca (C.A.S.), howard.lipshitz@utoronto.ca (H.D.L.)
https://doi.org/10.1016/j.celrep.2020.02.066

SUMMARY

G3BP RNA-binding proteins are important components of stress granules (SGs). Here, we analyze the role of the *Drosophila* G3BP Rasputin (RIN) in unstressed cells, where RIN is not SG associated. Immunoprecipitation followed by microarray analysis identifies over 550 mRNAs that copurify with RIN. The mRNAs found in SGs are long and translationally silent. In contrast, we find that RIN-bound mRNAs, which encode core components of the transcription, splicing, and translation machinery, are short, stable, and highly translated. We show that RIN is associated with polysomes and provide evidence for a direct role for RIN and its human homologs in stabilizing and upregulating the translation of their target mRNAs. We propose that when cells are stressed, the resulting incorporation of RIN/G3BPs into SGs sequesters them away from their short target mRNAs. This would downregulate the expression of these transcripts, even though they are not incorporated into stress granules.

INTRODUCTION

Post-transcriptional regulation (PTR) plays a key role in the control of gene expression in all cell types (Bovaird et al., 2018; Tutucci et al., 2018). PTR is achieved by RNA-binding proteins (RBPs) and small RNAs, such as microRNAs (miRNAs), which act as specificity factors that modulate the interaction of mRNAs with the cellular machinery that localizes, translates, and degrades mRNAs (Achsel and Bagni, 2016; Iadevaia and Gerber, 2015; Van Treeck and Parker, 2018).

PTR is particularly important in early animal embryos, where maternally provided mRNAs and proteins control developmental events prior to transcriptional activation of the embryo's genome (Tadros and Lipshitz, 2009; Vastenhouw et al., 2019). In several model animals, including *Drosophila*, the transfer of control from maternal products to those synthesized by the embryo's own genome—the maternal-to-zygotic transition (MZT)—is very rapid, occurring over a matter of hours, and thus facilitating studies of the mechanisms and functions of PTR. For example, it has been shown that the *Drosophila* RBP Smaug (SMG), which binds to specific stem-loop structures in its target mRNAs to repress their translation and trigger their degradation (Aviv et al., 2003, 2006; Chen et al., 2014; Semotok et al., 2005, 2008; Smibert et al., 1996, 1999), is essential for repression and clearance of hundreds of maternal mRNAs and for timely activation of the zygotic genome (Benoit et al., 2009; Laver et al., 2015b; Luo et al., 2016; Tadros et al., 2007). SMG is not the only negative regulator of maternal transcripts in *Drosophila*; additional RBPs (e.g., brain tumor; Laver et al., 2015a) or miRNAs (e.g., miR-309; Bushati et al., 2008) function in maternal mRNA clearance.

PTR also serves as a rapid response to cellular stress. Under stress conditions, cells shut down translation of many mRNAs while upregulating transcription and/or translation of sets of protein chaperones that maintain basal cellular integrity. Repression occurs, at least in part, in membraneless organelles known as stress granules (SGs) (Harvey et al., 2017; Panas et al., 2016; Protter and Parker, 2016; Van Treeck and Parker, 2018). SGs are thought to contain transcripts that are stalled in translation initiation (Anderson and Kedersha, 2009a, 2009b; Buchan and Parker, 2009; Kedersha and Anderson, 2009), and recent global analyses have shown that SGs are enriched for long transcripts (Khong et al., 2017; Namkoong et al., 2018).

An important component of SGs is the RBP G3BP, which is conserved throughout eukaryotes. Mammals have two genes, G3BP1 and G3BP2, whereas in *Drosophila* there is a single gene, *Rasputin* (*rin*). In human cells, G3BPs are necessary for SG formation, and if overexpressed, they are sufficient to induce SGs even in the absence of stress (Tourrière et al., 2003). RIN is necessary for SG formation in the *Drosophila* S2 tissue culture cell line, and although RIN or G3BP overexpression can induce

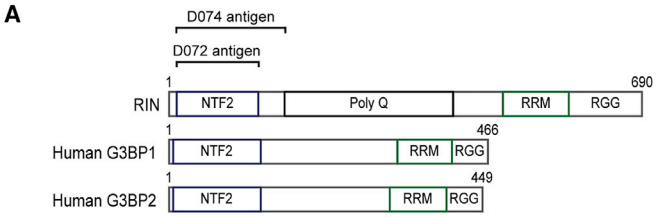

B

	Total RIN peptide counts (3 replicates)	
	RIN IP	Control IP
(-) RNase	682 | 554 | 1012	5 | 0 | 13
(+) RNase	1048 | 662 | 1214	8 | 0 | 0

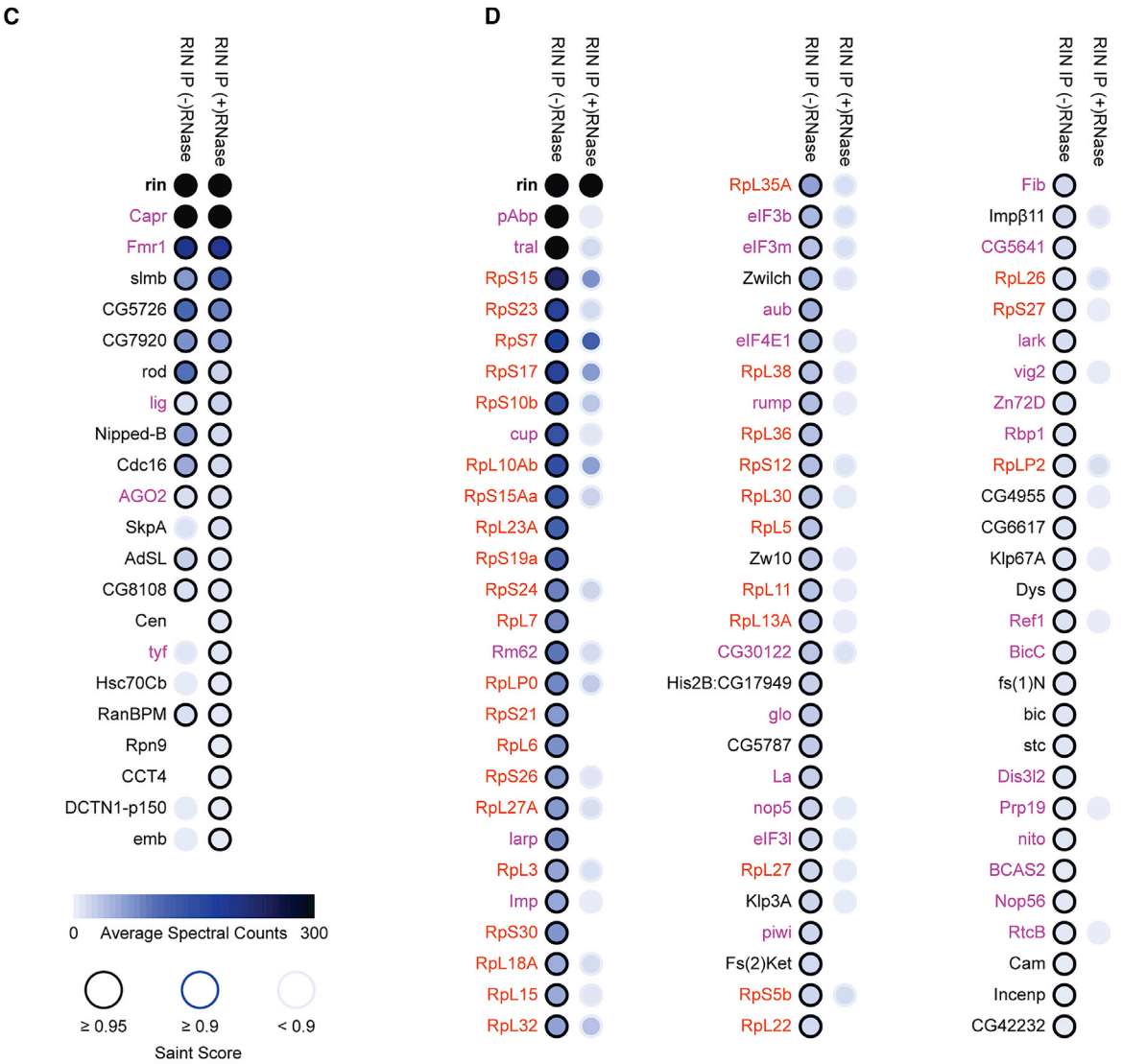

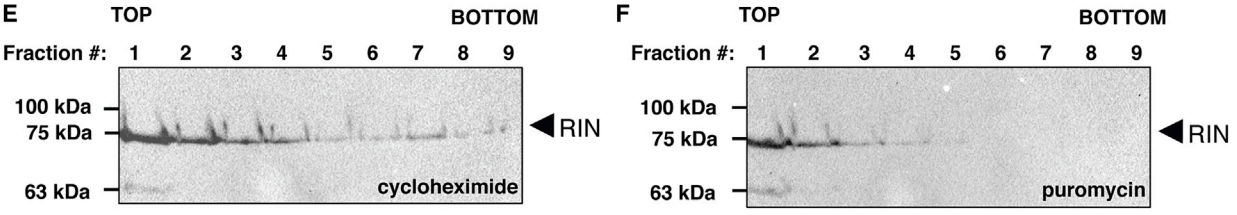

(legend on next page)

SGs in human cells, this is not the case in S2 cells (Aguilera-Gomez et al., 2017). RIN and G3BPs interact with several of the same protein partners under both stress and non-stress conditions; these include Caprin (CAPR), FMRP (FMR1 in *Drosophila*), and UPA2 (Lingerer [LIG] in *Drosophila*) (Aguilera-Gomez et al., 2017; Baumgartner et al., 2013; Costa et al., 2013; Jain et al., 2016; Kedersha et al., 2016; Markmiller et al., 2018; Youn et al., 2018).

The roles of RIN/G3BPs in unstressed cells have received less attention than their roles upon stress. Multiple functions have been attributed to G3BPs (reviewed in Alam and Kennedy, 2019), including transcript destabilization and repression (e.g., *c-myc*, *BART*, *CTNNB1*, *PMP22*, *HIV-1*, and *miR-1*), transcript stabilization (e.g., *Tau* and *SART3*), subcellular transcript localization (e.g., *Twist1*), and transcript sequestration into virus-induced foci (e.g., *HIV-1*). In *Drosophila*, mutations in the *rin* gene cause severe defects in oogenesis, mutant females lay few eggs, and those that are laid fail to hatch (Costa et al., 2013). *rin* mutations can also result in tissue patterning and growth defects (Baumgartner et al., 2013; Pazman et al., 2000). Despite RIN's essential function in the fly life cycle, there have been no analyses of the RIN-bound transcriptome or RIN's global role in gene regulation, nor are the molecular mechanisms that underlie RIN function known.

To better understand the function of RIN/G3BP in unstressed cells, we have carried out global analyses of the RIN-associated proteome and transcriptome in early *Drosophila* embryos. Using an anti-RIN synthetic antibody that we isolated from a phage-displayed library of fragments antigen binding (Fab) (Na et al., 2016; Persson et al., 2013), we immunoprecipitated RIN and then carried out mass spectrometry (IP-MS) to identify RIN's partner proteins. Interactions were found with several RBPs previously shown to interact with G3BP/RIN (e.g., CAPR, FMR1, and LIG), consistent with IP of a biologically relevant RIN-containing complex. RNA-dependent interactions with RIN were found for both small and large ribosomal subunit proteins, suggesting that RIN may be polysome associated, a fact that we confirmed using polysome gradients. By coimmunoprecipitating RIN together with bound mRNAs followed by microarray analysis, we identified hundreds of *in vivo* target transcripts in embryos, which are characterized by two features: they are short and enriched for a binding motif that was previously identified *in vitro* (Cook et al., 2011; Ray et al., 2013). RIN-associated mRNAs are enriched for Gene Ontology (GO) terms for core components of the transcription, splicing, and translation machinery as well as of mitochondria. RIN's endogenous targets in early embryos are more stable and more highly translated than co-expressed unbound transcripts. Their shorter length and higher rates of translation contrast with the behavior of mRNAs associated with SGs. Consistent with a role for RIN as a positive regulator of transcript stability, in *rin* mutants, the abundance of several highly bound target mRNAs is reduced relative to controls. Using a heterologous RNA-binding domain to tether RIN, G3BP1, or G3BP2 to a luciferase reporter mRNA in S2 tissue culture cells, we confirmed that RIN/G3BP increases the stability and/or translation of bound transcripts in the absence of stress.

Our data support a conserved function for G3BP proteins as potentiators of the translation and stability of their target transcripts. We speculate that stress-dependent recruitment of G3BPs/RIN into SGs may serve as a mechanism to downregulate gene expression both directly, by removing RIN from its endogenous target mRNAs, as well as indirectly, through reduced transcription, splicing, and translation.

RESULTS

Expression of RIN in Early Embryos

We analyzed endogenous RIN expression in early embryos by western blots and whole-mount immunofluorescence. The expression level of RIN does not change significantly through the time course examined (0–4 h; Figures S1A and S1B). RIN is enriched in the cortex of the early embryo, is concentrated apical to the nuclei at the syncytial blastoderm stage (Figures S1C–S1F), and is not present in foci. We compared the distribution of RIN with a known interacting protein, FMR1 (Monzo et al., 2006), and found that their distributions overlap in the cortex (Figures S1C–S1E). This pattern for RIN is consistent with previously published data on the *Drosophila* ovary showing that RIN is enriched in the cortical cytoplasm of the nurse cells and the oocyte (Costa et al., 2013).

RBPs, Translation Factors, and Ribosomal Proteins Co-purify with RIN, which Exhibits Polysome Association

To identify protein partners and mRNA targets of RIN in early embryos, an anti-RIN synthetic antibody, D072, was generated against its NTF2-like domain (Figure 1A) and was used to IP endogenous RIN from 0- to 3-h-old embryos followed by mass spectrometry (liquid chromatography-tandem mass spectrometry [LC-MS/MS]). To differentiate proteins that associate with RIN by protein-protein interactions versus through co-binding to RIN's target RNAs, IPs were performed, respectively, in the presence (+) or absence (–) of RNase A. In both cases, RIN

Figure 1. RIN Interacts with Multiple RNA-Associated Proteins in Early Embryos and Is Polysome Associated

(A) The domain structure of *Drosophila* RIN and its human orthologs G3BP1 and G3BP2. Synthetic antibodies used in this study were generated against antigens encompassing the NTF2 domain, as indicated.

(B) Total RIN peptide counts in IPs using the anti-RIN antibody D072 or the C1 control antibody.

(C and D) RIN IP-MS results depicted using the ProHits-viz web server (Knight et al., 2017). Shown are proteins identified as RIN interactors with a SAINT score of $\geq$0.95 and BFDR of $\leq$0.01. In (C) are proteins identified as RNA-independent interactors and in (D) as RNA-dependent interactors. The shade of the dot fill represents protein abundance in the RIN IPs minus control IPs, based on total peptide counts, and the shade of the dot outline represents the SAINT score, as indicated in the legend at the bottom of (C). Protein names highlighted in magenta are known RBPs, mRNP complex components, or translation factors, and orange highlighting indicates ribosomal proteins.

(E and F) Embryo extract treated with either cycloheximide (E) or puromycin (F) was fractionated on sucrose gradients, with the resulting fractions assayed for RIN by western blot.

See also Figures S1 and S2 and Table S1.

was among the most abundant proteins identified and was greatly enriched in anti-RIN IPs compared with those performed with a control synthetic antibody, C1 (Laver et al., 2012, 2013, 2015a; Na et al., 2016; Figure 1B).

We performed significance analysis of interactome (SAINT; Choi et al., 2011) and defined RIN interactors as proteins that were significantly enriched in the RIN IPs with a SAINT score of $\geq$0.95 and a Bayesian false discovery rate (BFDR) of $\leq$0.01. In addition to RIN itself, 21 proteins were enriched in the (+) RNase IPs and 96 proteins were enriched in the (–) RNase IPs (Figures 1C and 1D; Table S1).

Consistent with a role for RIN in PTR in the early embryo, of the total of 104 proteins identified in our RIN IPs, 68% (71) are known to be involved in post-transcriptional processes (as annotated by FlyBase Release FB2019_06; http://flybase.org/): 36 of them are known RBPs, mRNP complex components, or translation factors (Figures 1C and 1D, highlighted in magenta), and 35 are ribosomal proteins (Figures 1C and 1D, highlighted in orange), including 36% of the small subunit and 39% of the large subunit proteins (14 of 39 and 21 of 54, respectively) (Marygold et al., 2007). Overall, 92% (66) of the RBPs and ribosomal proteins that co-purified with RIN did so in an RNA-dependent manner, including all of the 40S and 60S subunit proteins.

Previous studies have identified sets of RIN/G3BP-interacting proteins in other contexts and species. In *Drosophila* ovaries, RIN has been shown to be in an RNase-resistant complex with ORB (Costa et al., 2005); ORB is absent from embryos (Hafer et al., 2011) and, therefore, did not coIP in our experiments. Another mass spectrometric analysis, which used Dorsal (DL) as a negative control, identified additional RIN-interacting proteins in ovaries (Costa et al., 2013). In that study, of the proteins that they found to IP with RIN but not DL, eight were also present on our early embryo lists: three were RNA independent (FMR1, LIG, and Twenty-four [TYF]) and four were RNA dependent (PABP, RpS24, RpL11, and RpL13A). An additional nine proteins on our lists were found in both their RIN and their DL IPs: one (CAPR) was on our RNA-independent list, and eight were on our RNA-dependent list (Trailer-hitch [TRAL], Cup, Fibrillarin [FIB], RpL3, RpL15, RpLP0, RpLP2, and RpS5).

Human G3BPs interact with many of the same proteins in both unstressed and stressed cells (Jain et al., 2016; Markmiller et al., 2018; Youn et al., 2018). We, therefore, compared our list of RIN interactors with G3BP interactors and SG components identified in recent global proteomic analyses in human and yeast cells (Jain et al., 2016; Markmiller et al., 2018; Solomon et al., 2007; Youn et al., 2018; Jain et al., 2016; Table S1). A total of 24% (5/21) of RIN's RNA-independent and 25% (24/96) of the RNA-dependent interactors were identified as G3BP interactors in the human datasets. Regarding RIN's RNA-independent interactors, all of the human datasets included CAPR, FMR1, and LIG, and one study (Jain et al., 2016) found two additional proteins that were on our RNA-independent list (HSC70Cb and DCTN-p150). Seven of the proteins on our RNA-dependent list overlapped with budding yeast SG components (PABP, TRAL, LARP, RUMP, eIF3b, eIF4E1, and RpS30). Regarding our RNA-dependent list, 84% of the proteins that overlapped with the human or yeast datasets are RBPs or translation factors (21/25).

G3BP interacts with the 40S (but not the 60S) ribosomal subunit in the context of SGs and their formation (Kedersha et al., 2016). Surprisingly, our data showed that RIN interacts with multiple proteins from both the 40S and 60S subunits. Because these RIN interactions were RNase sensitive, one possibility is that, in early embryos, RIN binds to mRNAs that are actively translated, and thus the ribosomes transiting these mRNAs co-purify with RIN. To assess whether RIN is associated with polysomes, we ran early embryo extracts on sucrose gradients treated with cycloheximide (which stabilizes the interaction of ribosomes with mRNAs) or puromycin (which disrupts mRNA-ribosome associations), followed by western blotting with an anti-RIN antibody (Aguilera-Gomez et al., 2017; Figures 1E–1F, and S2). These experiments showed that a subset of RIN is polysome associated.

Taken together, our data confirm that numerous RIN/G3BP-partner protein interactions occur under both non-stress and stress conditions and are conserved in *Drosophila*, yeast, and human cells. Furthermore, unlike in stressed cells, in early embryos RIN is found on polysomes.

RIN Associates with Hundreds of mRNA Species in the Early Embryo

To identify mRNAs associated with RIN in 0- to 3-h embryos, we used the D072 anti-RIN synthetic antibody to carry out RNA coIPs followed by microarray analysis (RNA coIP-microarray [RIP-Chip]). Significance analysis of microarrays (SAM) (Tusher et al., 2001) identified the mRNAs encoded by 566 genes that were enriched at least 2-fold and with an FDR <5% in RIN IPs compared with control IPs performed with the C1 antibody. We defined these as RIN-associated mRNAs (Figure S3; Table S2).

We validated our set of RIN-associated transcripts in two ways. First, we performed two additional biological replicate RIPs by using the anti-RIN antibody (D072) and control antibody described above, after which quantitative reverse-transcriptase PCR (qRT-PCR) was used to quantify five highly enriched RIN-associated mRNAs and four mRNAs not associated with RIN according to our RIP-Chip experiments. The RIN-associated mRNAs were 2- to 7-fold more enriched in the RIN versus control RIP-qRT-PCR than were the non-target mRNAs (Figure S3). Second, we generated an additional synthetic antibody, designated D074, against the NTF2-like domain of RIN (Figure 1A), which we used to perform RIP-Chip, and compared the average fold enrichment (FE) of transcripts in the initial anti-RIN D072 RIP-Chip to the FEs in the RIP-Chip performed with D074. The results were consistent with the initial RIP-Chip data, with a Spearman correlation rho value for the comparison of FEs of 0.79 ($p < 10^{-15}$) (Figure S3).

RIN-Associated mRNAs Are Short and Enriched for the *In Vitro* Binding Motif of the RIN RNA Recognition Motif (RRM)

Next, we assessed the properties of RIN-associated transcripts. Strikingly, we found that RIN-associated mRNAs in early embryos are significantly shorter than co-expressed unbound transcripts with the area under the receiver operating characteristic (AUROC) = 0.83 ($p < 10^{-10}$; Figure 2A). The ROC graphs the

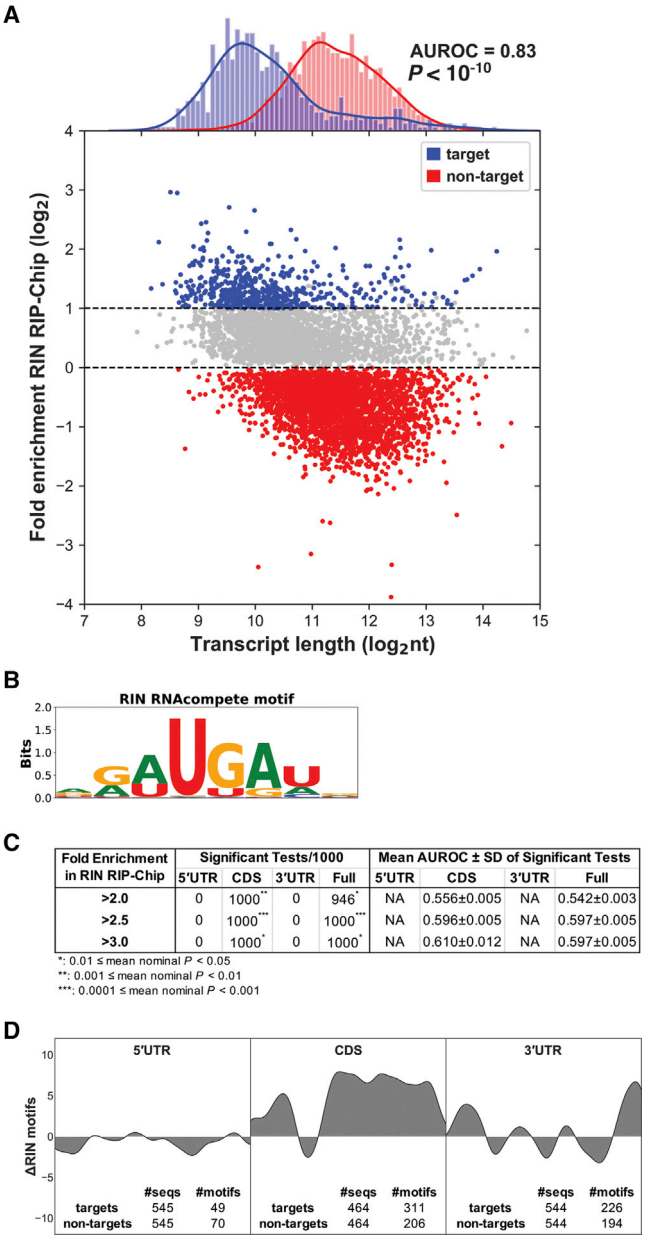

Fold Enrichment in RIN RIP-Chip	Significant Tests/1000				Mean AUROC ± SD of Significant Tests			
	5′UTR	CDS	3′UTR	Full	5′UTR	CDS	3′UTR	Full
>2.0	0	1000**	0	946*	NA	0.556±0.005	NA	0.542±0.003
>2.5	0	1000***	0	1000***	NA	0.596±0.005	NA	0.597±0.005
>3.0	0	1000*	0	1000*	NA	0.610±0.012	NA	0.597±0.005

*: 0.01 ≤ mean nominal $P < 0.05$
**: 0.001 ≤ mean nominal $P < 0.01$
***: 0.0001 ≤ mean nominal $P < 0.001$

Figure 2. RIN-Associated Transcripts Are Short and Enriched for the RIN RRM's *In Vitro* Binding Motif

(A) Plot showing the relationship between transcript length and association with RIN, for all genes with transcripts represented on the microarray that were defined as expressed in early embryos. Transcript length for each gene is taken to be the length of the longest annotated transcript isoform, and RIN association is represented by the fold enrichment in the RIN RIP-Chip versus control RIP-Chip of the most highly enriched probe set on the microarray for each gene. Genes encoding RIN-associated transcripts (enriched >2-fold in RIN versus C1 RIP, FDR <5%) are highlighted in blue. Co-expressed RIN non-targets (defined as $\log_2$ fold enrichment in RIN versus C1 RIPs of <0) are highlighted in red. Gene length distributions of RIN targets and non-targets are shown in the density plots at the top. AUROC and p value of Mann-Whitney U test on lengths of RIN targets and non-targets are shown.

(B–D) The *in vitro* RIN motif from RNAcompete (Ray et al., 2013) shown in (B) is significantly enriched in the coding sequences of RIN-associated mRNAs (C and D). (C) Table showing the number, AUROC, and range of nominal p values of significant tests out of 1,000 trials with randomly selected targets and length-paired non-targets. (D) Plot showing the difference in number of RIN motifs in the 3′ UTR, CDS, and 5′ UTR of RIN-associated transcripts versus randomly selected co-expressed length-paired RIN non-targets for each region. The total number of RIN motifs (defined as sites with "hit score" of >0.001) in targets and non-targets for each region are grouped into 20 bins. The difference between the two Gaussian kernels fitting the motif distribution of targets and non-targets for each region is displayed on the plot. The locations of motifs are represented by the relative location of the first nucleotide in the corresponding region.

See also Figures S3, S4, and S6 and Tables S2 and S3.

diagnostic ability of a binary classifier by plotting the true-positive rate versus the false-positive rate; no diagnostic ability gives an AUROC of 0.5 and perfect ability gives an AUROC of 1.0. For the Mann-Whitney *U* test, the AUROC is equivalent to the *U* statistic divided by the product of the numbers of targets and non-targets.

To assess whether enrichment of short mRNAs might be an artifact of our RIP-Chip method, we reanalyzed our previously published data for three other RBPs—Brain tumor, Pumilio, and Staufen (endogenous Staufen and transgenic GFP-Staufen)—for which we used the same method and microarray platform (Laver et al., 2013, 2015a). For all four RIP-Chip datasets, in contrast to the RIN dataset, there was either enrichment for long mRNAs relative to co-expressed unbound transcripts (Figures S4A, S4B, and S4D) or no length difference (Figure S4C). We conclude that short mRNAs do indeed co-purify with RIN.

To identify additional features of RIN-associated mRNAs, we performed *de novo* motif discovery using #ATS (Number of Accessible Target Sites), a discriminative tool that searches for sequence motifs that are enriched in targets versus non-targets (Li et al., 2010). We failed to discover a consistent and significant motif in RIN targets compared with length-matched co-expressed non-targets (Table S3).

RIN and G3BP-binding motifs have been reported from *in vivo* (Edupuganti et al., 2017) and *in vitro* (Cook et al., 2011; Ray et al., 2013) studies. To assess whether any of these motifs were enriched in RIN-associated mRNAs, we used position frequency matrices (PFMs) from those studies together with RNAplfold, where the latter was used to define motif matches that were single-stranded and, thus, available for RBP binding (Bernhart et al., 2006; Li et al., 2010). For each motif, we tested its ability to distinguish RIN-associated (positive) transcripts from length-paired, co-expressed, non-RIN-associated (negative) transcripts by ranking transcripts with the maximum "hit score" achieved for that motif, across all subsequences of a transcript (i.e., the best possible subsequence resembling the motif sequence in a context that is predicted to be single stranded). We performed this test by using three RIN fold-enrichment (FE) cutoffs (>2, >2.5, and >3) and four transcript regions (5′ untranslated region [UTR], coding sequence [CDS], 3′ UTR, and full mRNA), and we repeated each FE and region pair 1,000 times, with length-matched negatives randomly selected each time. We assessed how well the four motifs performed on samples from each FE cutoff and transcript region by the number of Mann-Whitney *U* tests that were significant (with $p < 0.05$) and the mean and standard deviation of the AUROC. We found that the *in vitro* RIN motif (Figure 2B) was significantly enriched in RIN-associated full

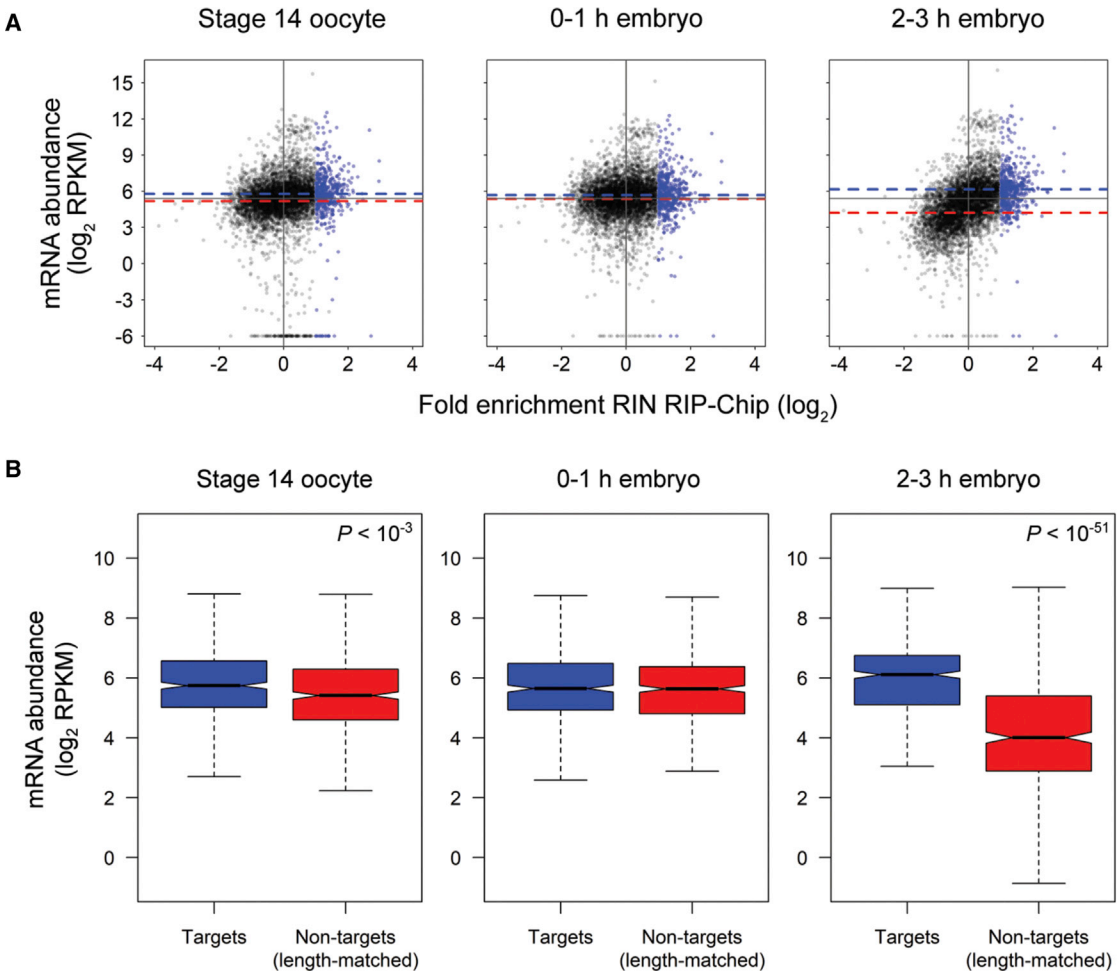

Figure 3. RIN-Associated Transcripts Are Stable during the Maternal-to-Zygotic Transition

(A) Plots showing the relationship between fold enrichment in the RIN RIP-Chip and mRNA levels measured by Eichhorn et al. (2016) during time points spanning the maternal-to-zygotic transition. RIN-associated transcripts are highlighted in blue. Dashed blue horizontal lines indicate median value of mRNA levels for RIN-associated transcripts at each time point, and dashed red horizontal lines indicate median values for RIN non-targets (log_2 fold enrichment in RIN versus C1 RIPs of <0) at each time point. For all time points, solid dark-gray horizontal lines indicate the median values of mRNA levels in stage 14 oocytes, as a reference, and solid vertical lines indicate no enrichment in the RIN RIP-Chip. Points are shown for all genes measured in both this study and Eichhorn et al. (2016) with the RIP-Chip fold enrichment value for each gene represented by the most highly enriched probe set on the microarray for that gene.

(B) Boxplots comparing mRNA levels, measured by Eichhorn et al. (2016), of RIN-associated transcripts ("targets"; blue) and a set of randomly selected, length-matched, co-expressed non-RIN-targets (red), for each time point depicted in (A). For comparisons with a statistically significant difference in mRNA levels between targets and length-matched non-targets, Wilcoxon rank-sum test p values are indicated in the top right of the plots.

See also Figure S5 and Tables S3 and S4.

mRNA sequences and was most enriched in the open reading frame (Figures 2C and 2D; Table S3). None of the motifs for the human G3BPs—defined either *in vitro* or *in vivo*—was enriched (Table S3).

We conclude that the major feature of RIN binding *in vivo* is short transcript length (AUROC = 0.83) with an additional, more minor, contribution from the motif (AUROC, 0.55 to 0.61).

RIN-Associated mRNAs Are Stable, Translated, and Depleted for SMG Recognition Elements

To gain insight into the effect RIN might have on the expression of its target mRNAs, we examined datasets that define the translational status (determined by ribosome occupancy) and abundance of the *Drosophila* transcriptome during late oogenesis and early embryogenesis and asked whether RIN association correlated with any particular post-transcriptional outcomes.

First, we examined the abundance of RIN-bound mRNAs and of co-expressed, unbound mRNAs (Eichhorn et al., 2016). The median abundance of these two classes of transcripts was similar in mature oocytes and 0- to 1-h embryos, whereas there was a striking change moving from 0- to 1-h embryos to 2- to 3-h embryos: non-target mRNAs significantly decreased in abundance (2.2-fold decrease in median reads per kilobase per million [RPKM]; Wilcoxon rank-sum test, $p < 10^{-150}$), whereas levels of RIN-associated transcripts increased significantly (1.4-fold increase in median RPKM; Wilcoxon rank-sum test,

$p < 10^{-3}$) (Figure 3A). This difference was maintained in 3- to 4- and 4- to 5-h embryos (Figure S5). Because RIN-associated mRNAs are short, we also carried out abundance analyses relative to length-matched non-targets and found that RIN-bound mRNAs are more stable at 2–3 h even when length is considered (Figure 3B; Table S4).

The first 3 h of embryogenesis encompass most of the *Drosophila* MZT, during which many maternally supplied mRNAs are degraded and the zygotic genome becomes transcriptionally active (Tadros and Lipshitz, 2009; Vastenhouw et al., 2019). Transcripts present in the early embryo have been classified according to their maternal and/or zygotic origin, as well as their patterns of stability or decay (De Renzis et al., 2007; Tadros et al., 2007; Thomsen et al., 2010). To understand how the abundance of RIN-associated transcripts described above reflects changes in levels of maternal or zygotic mRNAs, we compared RIN-associated mRNAs to these various classes. RIN-associated transcripts were enriched for two of these classes: maternally supplied transcripts that remain stable through the MZT and are not transcribed in the embryo (class I in Thomsen et al., 2010; Fisher's exact test, $p < 10^{-11}$; odds ratio, 2.0) and maternally supplied transcripts that remain stable and are also zygotically transcribed ("Stable + transcription" in Thomsen et al., 2010) (Fisher's exact test, $p < 10^{-27}$; odds ratio, 3.2). However, RIN-associated mRNAs were strongly depleted for maternally supplied transcripts that are degraded (classes II–V in Thomsen et al., 2010) (Fisher's exact test, $p < 10^{-48}$; odds ratio, 0.24), including those that are degraded and subsequently re-transcribed (class III in Thomsen et al., 2010) (Fisher's exact test, $p < 10^{-7}$; odds ratio, 0.20). Examination of two additional datasets, which defined mRNAs that are maternally supplied and degraded, also revealed depletion of RIN-associated mRNAs among transcripts that are degraded in unfertilized eggs (Tadros et al., 2007) (Fisher's exact test, $p < 10^{-17}$; odds ratio, 0.26) or in early embryos (De Renzis et al., 2007) (Fisher's exact test, $p < 10^{-54}$; odds ratio, 0.12). Thus, the dynamics of RIN-associated transcript levels in early embryos, described above, largely reflect RIN binding to stable, maternally supplied transcripts.

To assess the translational efficiency of RIN-associated mRNAs, we used a dataset that measured this parameter using ribosome occupancy (Eichhorn et al., 2016). This revealed that RIN-associated mRNAs had a significantly higher translational efficiency than co-expressed, non-target mRNAs, consistent with a role for RIN in potentiating translation. The largest and most significant difference was in 0- to 1-h embryos where the median translational efficiency of RIN-associated mRNAs was 4-fold higher than that of non-target mRNAs (dashed blue and red lines, respectively, in Figure 4A; Wilcoxon rank-sum test, $p < 10^{-100}$). The translational efficiency of RIN-associated mRNAs showed a significant increase moving from mature oocytes to 0- to 1-h embryos (1.6-fold increase; Wilcoxon rank-sum test, $p < 10^{-17}$), whereas the translational efficiency of co-expressed, non-target mRNAs decreased over the same stages. At earlier stages of oogenesis (stages 11–13) as well as at later embryonic time points (3–4 and 4–5 h), RIN-bound transcripts also consistently exhibited higher translational efficiency than co-expressed unbound transcripts (Figure S5). The positive correlation between an mRNA's association with RIN and its translational activity were supported by comparisons to an additional dataset that used ribosome occupancy to assess transcriptome-wide mRNA translation in early embryos (Dunn et al., 2013) (Figure S5). Because RIN-associated mRNAs are short, we also carried out analyses of translational efficiency relative to length-matched non-targets and found that RIN-bound mRNAs have higher translational efficiency at all time points even when length is considered (Figure 4B; Table S4).

The SMG RBP, which binds hairpin structures known as SMG recognition elements (SREs), is a well-characterized negative regulator of both mRNA stability and translation (Chen et al., 2014; Pinder and Smibert, 2013; Semotok et al., 2005, 2008; Smibert et al., 1996; Tadros et al., 2007). Because RIN-bound mRNAs are stable and translated in early embryos, we assessed whether they might be depleted for SREs. We calculated an SRE "score" (Chen et al., 2014) for RIN-associated mRNAs relative to length-matched, co-expressed, unbound mRNAs and found that RIN-bound mRNAs were strikingly depleted of SREs (Table S3).

A final feature that we examined was N^6-methyladenosine (m^6A) modification of RIN's targets because it has been reported that m^6A "repels" G3BP1 binding (Edupuganti et al., 2017). If so, then RIN-bound transcripts would be expected to be depleted for m^6A. We compared RIN-bound transcripts to m^6A modifications that were mapped transcriptome wide in 0- to 45-min, 45- to 90-min, and 1.5- to 6-h embryos (Kan et al., 2017). In all cases and for all transcript regions (5′ UTR, CDS, and 3′ UTR), there was neither significant enrichment nor significant depletion of m^6A-modified transcripts among RIN's targets (Fisher's exact test p values ranged from 0.15 to 1). We conclude that there is no evidence for a role—either positive or negative—of m^6A in determining RIN targets in early embryos.

Taken together, our data support a model in which RIN binds to maternally supplied transcripts, stabilizes them, and potentiates their translation.

RIN-Associated Transcripts in the Early Embryo Do Not Exhibit Properties of SG Transcriptomes

Human and yeast SG transcripts are long (Anderson and Kedersha, 2009a, 2009b; Buchan and Parker, 2009; Kedersha and Anderson, 2009; Khong et al., 2017; Namkoong et al., 2018), whereas RIN-associated mRNAs in early embryos are short. The high levels of translation of RIN-associated transcripts in the early *Drosophila* embryo also contrast with the translationally silent transcripts found together with G3BPs in SGs (Anderson and Kedersha, 2009a, 2009b; Buchan and Parker, 2009; Kedersha and Anderson, 2009).

To ask whether the RIN-associated transcripts are likely to be recruited to SGs or, instead, represent a separate pool of RIN-associated mRNAs, we compared our list of RIN-associated mRNAs to the *Drosophila* homologs of transcripts found to be either enriched in or depleted from human U2OS SGs (Khong et al., 2017): RIN-associated *Drosophila* mRNAs were significantly depleted for homologous SG-enriched transcripts (Fisher's exact test, $p < 10^{-7}$; odds ratio, 0.45) but were enriched for SG-depleted transcripts ($p < 10^{-29}$; odds ratio, 3.2). Likewise, RIN-associated mRNAs were significantly depleted for transcripts homologous to those that undergo localization to RNA granules under endoplasmic reticulum (ER) stress (Fisher's exact

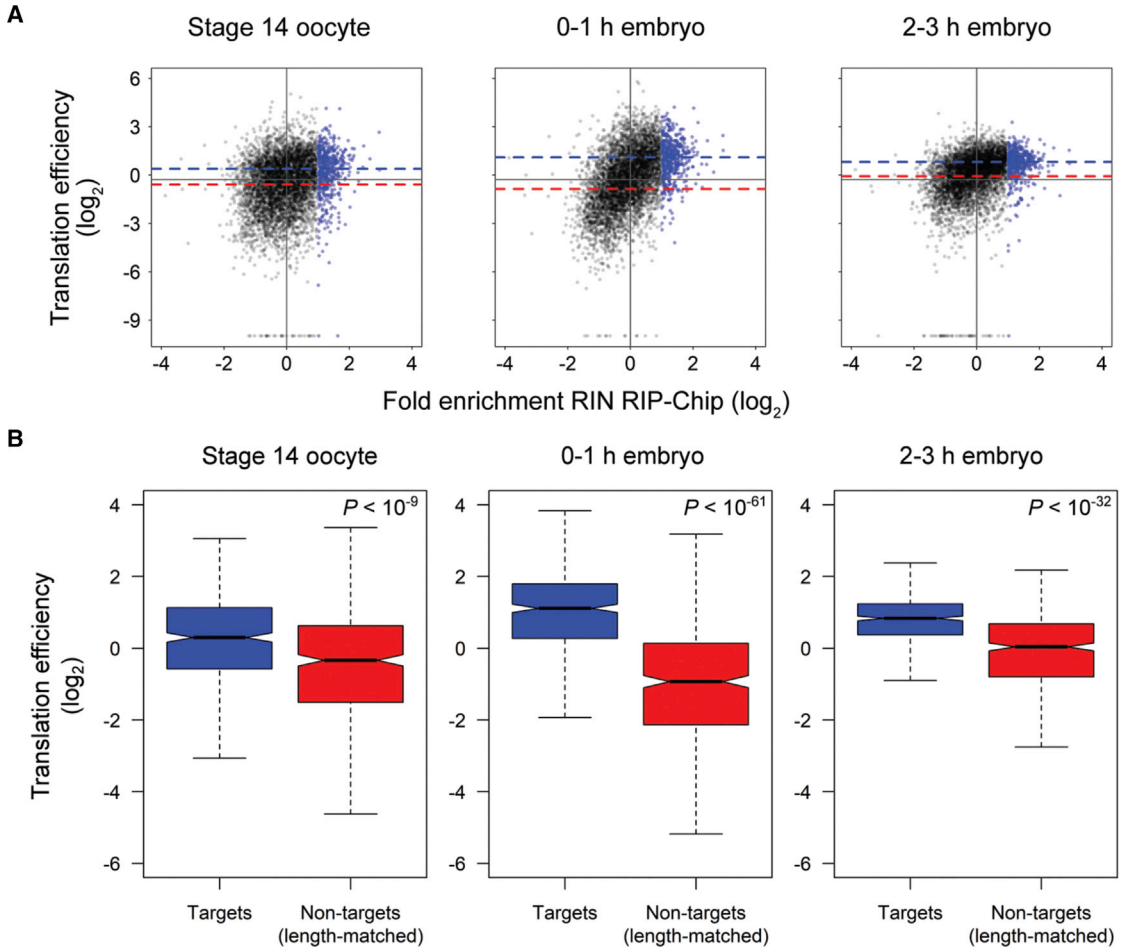

Figure 4. RIN-Associated Transcripts Are Highly Translated during the Maternal-to-Zygotic Transition

(A) Plots showing the relationship between fold enrichment in the RIN RIP-Chip and translational efficiency measured by Eichhorn et al. (2016) during time points spanning the maternal-to-zygotic transition. Color code is as in Figure 3 but with respect to translational efficiency rather than RNA abundance. For all time points, solid dark-gray horizontal lines indicate the median values of translational efficiency in stage 14 oocytes, as a reference, and solid vertical lines indicate no enrichment in the RIN RIP-Chip. Points are shown for all genes measured in both this study and Eichhorn et al. (2016), with the RIP-Chip fold enrichment value for each gene represented by the most highly enriched probe set on the microarray for that gene.

(B) Boxplots comparing translational efficiency, measured by Eichhorn et al. (2016) of RIN-associated transcripts ("targets"; blue) and a set of randomly selected, length-matched, co-expressed non-RIN-targets (red), for each time point depicted in (A). For comparisons with a statistically significant difference in translational efficiency between targets and length-matched non-targets, Wilcoxon rank-sum test p values are indicated in the top right of the plots.

See also Figure S5 and Table S4.

test, $p < 10^{-4}$; odds ratio, 0.49), heat shock (Fisher's exact test, $p < 10^{-7}$; odds ratio, 0.55), or arsenite treatment (Fisher's exact test, $p < 10^{-8}$; odds ratio, 0.49) in NIH 3T3 cells (Namkoong et al., 2018). The observed enrichment or depletion of these classes in RIN-bound transcripts is consistent with the fact that the fly homologs of SG-enriched or -depleted transcripts show the same length distribution as the human transcripts (Figure S6).

We also compared the length and translational efficiency of the *Drosophila* homologs of mammalian mRNAs that are either enriched in or depleted from SGs. There was no significant correlation of low translational efficiency and length of the fly homologs of SG-enriched transcripts, whereas there was a significant negative correlation between length and translational efficiency of the fly homologs of SG-depleted transcripts (Figure S6).

These analyses are consistent with the hypothesis that the transcripts with which RIN associates in early embryos are a separate pool from those typically found in SGs.

RIN-Associated mRNAs Encode Core Gene Expression and Mitochondrial Components

We next asked what biological and molecular functions RIN might control in early embryos by searching for GO terms enriched among the proteins encoded by the RIN-associated mRNAs, using the DAVID (Database for Annotation, Visualization and Integrated Discovery) functional annotation tool (Huang et al., 2009a, 2009b; Table 1; Table S5). This revealed a striking enrichment for roles in the regulation of gene expression and in mitochondrial function.

Table 1. Representative GO Terms Enriched among Proteins Encoded by RIN-Associated mRNAs

Enriched Function or Complex	Representative GO Terms	Fold Enrichment	FDR (%)
Oxidative phosphorylation	Oxidative phosphorylation (GO: 0006119)	4.32	2.80×10^{-5}
	Respiratory chain complex (GO: 0098803)	4.21	2.92×10^{-5}
Ribosome	Mitochondrial ribosome (GO: 0005761)	3.43	3.63×10^{-4}
	Cytosolic large ribosomal subunit (GO: 0022625)	2.65	5.81
Ragulator complex	Ragulator complex (GO: 0071986)	11.02	0.44
Transcription	DNA-templated transcription, initiation (GO: 0006352)	2.56	0.52
	Histone acetylation (GO: 0016573)	2.35	9.11
mRNA splicing	RNA splicing (GO :0008380)	1.75	1.78

Regarding the regulation of gene expression, RIN's targets included mRNAs encoding proteins involved in multiple levels of control, most notably transcription, pre-mRNA splicing, and translation. Among those involved in transcription were mRNAs encoding general transcription factors, including four subunits of the TFIID complex (*Taf1*, *Taf10b*, *Taf12*, and *Taf13*), both of the subunits of the TFIIA complex (*TfIIA-S* and *TfIIA-L*), six subunits of the "mediator" transcriptional co-activator complex (*MED4*, *7*, *11*, *21*, *26*, and *28*), histone modifiers, and transcription factors with important roles in the activation of zygotic transcription, such as *Zelda* and *Stat92E*. mRNAs associated with RIN that encode splicing-related factors included a number of spliceosome subunits as well as regulators of pre-mRNA splicing, such as *transformer* and *transformer 2*. With regard to translation, RIN-associated mRNAs were enriched for those encoding protein components of both the cytosolic ribosome (12 large subunit, 2 small subunit) and the mitochondrial ribosome (15 large subunit, 8 small subunit). In addition, mRNAs that encode all five subunits of the "Ragulator" complex were found to be RIN associated. Ragulator regulates activation of the target of rapamycin (TOR) pathway in response to amino acid availability (Bar-Peled et al., 2012; Sancak et al., 2010).

Regarding mitochondria, in addition to the transcripts encoding 23 mitochondrial ribosomal proteins, RIN was associated with 30 nuclear-encoded mRNAs for proteins that are either components of the mitochondrial respiratory chain complexes I to V or involved in their assembly. Additional mRNAs associated with RIN included those encoding components of the mitochondrial contact site and cristae-organizing system (MICOS) complex, which acts to maintain mitochondrial cristae and membrane architecture and FIS1, which has a role in promoting mitochondrial fission.

We next examined each of the GO-term-enriched classes in detail. Strikingly, we found that the vast majority of transcripts in each category tended to be enriched in the RIN IP, albeit not to the level of statistical significance (in Figure 5 compare transcripts associated with RIN, highlighted in blue, and transcripts that fell below the cutoff used to define RIN-associated mRNAs, highlighted in red). Notably, there was also a clear negative correlation between transcript length and RIN-binding in each GO term class (Figure 5), indicating that the correlation of RIN association with shorter transcript length is independent of the function of the bound mRNAs. Finally, the "red" transcripts in each GO term class tended to have similar translational efficiency and stability to the RIN-bound ("blue") transcripts in that class, albeit again not to as great an extent (Figure S7). These results suggest that RIN's role in binding and regulating mRNAs that encode core components of transcription, splicing, translation, and mitochondria is more pervasive than predicted from examination of only its most highly bound targets.

These analyses lead to the hypothesis that RIN plays a global role in binding and potentiating the stability and translation of mRNAs that encode core components of gene expression and mitochondria in early embryos.

Levels of RIN's Target Transcripts Are Reduced in *rin* Mutants

To assess the consequences of removal of endogenous RIN on the expression of RIN's target mRNAs, we produced females *trans*-heterozygous for two previously identified *rin* alleles, rin^2 (Pazman et al., 2000) and rin^3 (Costa et al., 2013) (i.e., of genotype rin^2/rin^3) and used as controls females that were either $rin^2/+$ or $rin^3/+$. We selected for analysis 13 mRNAs that were highly enriched in the RIP-Chip experiments, 5 that were unchanged, and 7 that were depleted (Table S6). We used qRT-PCR to analyze transcript levels in at least three biological replicates from ovaries rather than embryos to exclude secondary effects in embryos from the mutant (Costa et al., 2013). Expression was normalized to the average of the transcripts with no enrichment for RIN association, and the change in expression of the depleted, non-enriched, and enriched groups was compared pairwise between rin^2/rin^3 mutant ovaries and control ovaries by using the two-tailed Wilcoxon rank-sum test. Transcripts depleted for RIN binding and transcripts non-enriched for RIN binding did not show a significant change in expression in mutant ovaries compared with control ($z = 0.82$, $p = 0.41$ and $z = 0.12$, $p = 0.90$, respectively). In contrast, transcripts enriched for RIN binding showed a significant decrease in expression levels in mutant ovaries relative to the control ($z = 3.63$, $p < 3 \times 10^{-4}$) (Table S6). These data are consistent with the hypothesis that RIN acts as a potentiator of the stability of its maternal mRNA targets.

RIN and G3BP Potentiate mRNA Stability and Translation in S2 Tissue Culture Cells

Finally, to experimentally test the prediction that RIN is a potentiator of mRNA stability and translation, we tethered FLAG-tagged full-length RIN protein fused to a peptide of the bovine

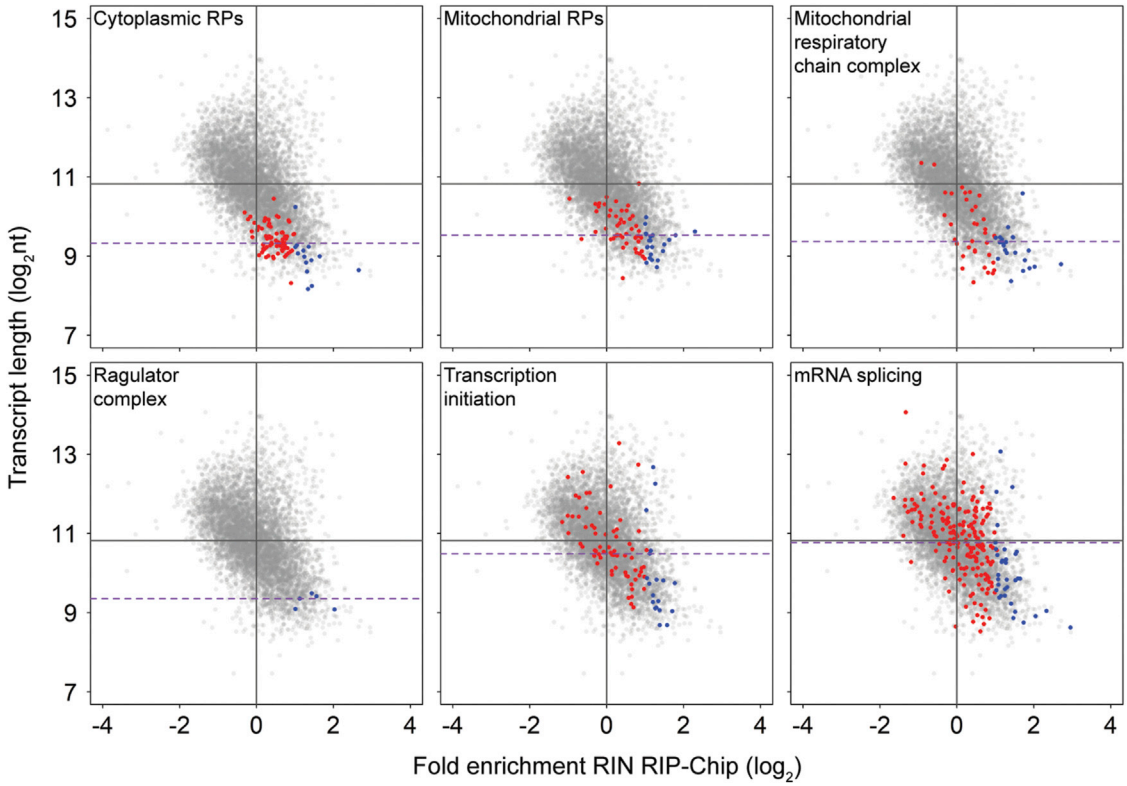

Figure 5. RIN Association with mRNAs Is Correlated with Shorter Transcript Length for All of the Enriched GO-Term Categories

Plots showing, for transcripts annotated with enriched GO terms, the relationship between length and association with RIN. Blue and red points represent genes annotated with the indicated GO term: genes associated with RIN are blue, and genes that fell below the cutoff used to define RIN-associated mRNAs are red. Dashed purple horizontal lines indicate the median transcript length for all genes annotated with a given GO term. Solid vertical lines indicate no enrichment in the RIN RIP, and solid dark-gray horizontal lines indicate the median length of all transcripts represented on the plot.

See also Figure S7 and Tables 1 and S5.

immunodeficiency virus transactivator protein (BIV-Tat) to a luciferase reporter mRNA containing six tandem BIV transactivation responsive (TAR) elements in its 3′ UTR (Wakiyama et al., 2012) in *Drosophila* S2 tissue culture cells (Figure 6A). BIV-Tat-FLAG-RIN behaved the same way as endogenous RIN (Aguilera-Gomez et al., 2017): under non-stress conditions it was ubiquitously distributed in the cytoplasm and co-localized with CAPR (Figure S1).

Tethering RIN resulted in a ~2.4-fold increase in luciferase protein levels compared with a negative control in which a BIV-Tat-FLAG-GFP fusion protein was tethered to the same reporter (Figure 6B). To determine whether this increase in luciferase levels might be a result of increased translation and/or increased mRNA levels, we also assayed luciferase mRNA levels. This revealed that RIN tethering resulted in a 1.9-fold increase in mRNA levels compared with the control (Figure 6C). These data show that RIN stabilizes the reporter mRNA.

We next assayed the expression levels of Tat-tagged RIN and GFP by western blot and found that GFP was expressed at significantly higher levels (Figure 6D). To assess whether the differential behavior of the TAR reporter in the presence of tethered RIN versus GFP could be explained by this difference in protein levels, we reduced the level of GFP plasmid transfected into cells, while keeping the levels of the RIN plasmid constant. This reduced the expression of GFP to levels equivalent to those seen for RIN (Figure 6E). When we compared luciferase expression in this experiment, the fold enhancement in luciferase expression mediated by tethered RIN was 3.4-fold (Figure 6F), confirming that tethered RIN enhances reporter expression.

To determine whether this might represent a conserved function of RIN, we tested the effect of tethering human G3BP1 or G3BP2 to the reporter mRNA in S2 cells. As was the case for BIV-Tat-FLAG-RIN, BIV-Tat-FLAG-G3BPs were ubiquitously distributed in the cytoplasm (Figure S1). Tethering either G3BP1 or G3BP2 led to increased levels of both luciferase protein and luciferase mRNA similar to those observed for RIN (Figures 6B and 6C). Thus, potentiation of mRNA stability and translation represent conserved functions of the RIN/G3BP family of proteins in unstressed cells.

DISCUSSION

Features of RIN-Bound Transcripts

Two features, short transcript length and the motif bound by the RIN RRM *in vitro*, are predictive of RIN binding. That short transcripts in general might be more likely to contain the motif

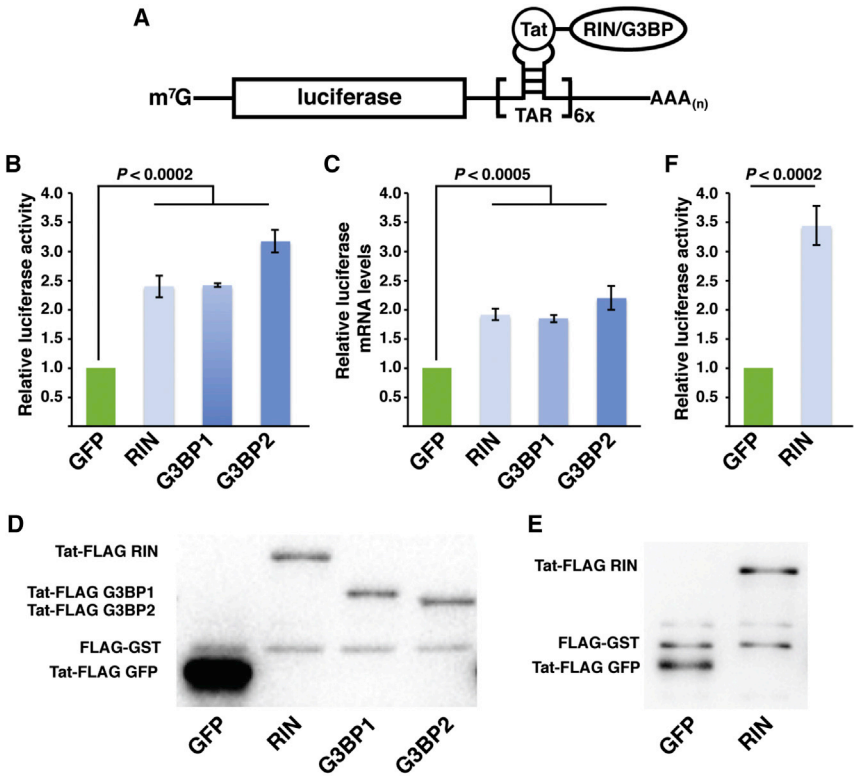

Figure 6. Tethering RIN or Its Human Homologs G3BP1 or G3BP2 Potentiates Reporter Expression

(A) A schematic representation of the tethering assay used to assess an RNA-binding protein's function. The *trans*-activator peptide (Tat) interacts with stem-loop structures known as *trans*-activation response (TAR) elements. By co-expressing a luciferase reporter mRNA carrying six TAR elements in the mRNA's 3′ UTR and RIN/G3BP-tagged Tat, RIN/G3BP is tethered to the luciferase mRNA.

(B) The Tat-tagged proteins indicated on the x axis were co-expressed in cells with TAR-tagged firefly luciferase mRNA. The y axis indicates the firefly luciferase enzyme activities normalized to a co-transfected unregulated *Renilla* luciferase. The normalized firefly luciferase enzyme activities for tethered RIN, G3BP1, or G3BP2 were compared to tethered GFP, whose normalized luciferase activity was set to 1 (n = 3).

(C) The relative firefly luciferase mRNA levels were assessed by qRT-PCR, when the protein indicated on the x axis was tethered. Firefly luciferase mRNA levels were normalized to *Renilla* luciferase mRNA levels and normalized GFP levels were set to 1 (n = 3).

(D) Tethered proteins carried a triple FLAG, allowing us to compare their levels using anti-FLAG western blots. Glutathione S-transferase (GST) carrying a triple FLAG tag served as a loading and transfection control.

(E and F) The same as (D) and (B), respectively, with the exception that the levels of transfected Tat-GFP were reduced 10-fold. In all graphs, error bars indicate standard deviation and results of Student's t tests are indicated.

See also Figure S1.

is excluded by the fact that RIN's target mRNAs are enriched for the motif compared with length-matched, co-expressed, unbound mRNAs. Thus, we propose that each feature separately contributes to RIN target mRNA binding, with shortness playing a greater role than the motif (AUROC = 0.83 and 0.55–0.61, respectively).

Although it is unclear how RIN is able to measure transcript length, there is a precedent for the differential behavior and regulation of short versus long mRNAs. For example, in general, short mRNAs are more highly translated than long mRNAs, and this is thought to reflect the fact that short mRNAs have a higher affinity for the cap-binding complex (Costello et al., 2015; Thompson and Gilbert, 2017). It has been proposed that this higher affinity is related to the possibility that short mRNAs are able to form a closed-loop structure more readily than longer mRNAs. We note that a recent study that calls the closed-loop model into question was unable to test short mRNAs because of technical limitations (Adivarahan et al., 2018). Thus, even if long mRNAs do not form a stable closed loop, it remains possible that short mRNAs do.

The ribosome-associated protein RACK1 has been shown to be required for the efficient translation of short but not long mRNAs (Thompson et al., 2016). Although we have shown here that RIN is associated with polysomes in early embryos, *Drosophila* RACK1 is not on our list of RIN protein interactors and neither is there a significant overlap between our RIN protein interaction network and a set of protein interactors previously identified for RACK1 (Kuhn et al., 2017). Thus, the mechanisms by which RIN recognizes short mRNAs may differ from those that have been identified previously.

Another striking feature of RIN-bound mRNAs is that they are depleted for SREs, the binding sites of SMG, which destabilizes and translationally represses its target mRNAs. This could suggest that the high translational efficiencies and stability of RIN-target mRNAs is simply a result of a lack of SREs. However, we have provided evidence that RIN can exert its effects in situations where the SMG protein is not present (i.e., during oogenesis, in embryos older than 3 h, and in S2 cells). Thus, we conclude that most RIN-bound mRNAs in the early embryo are upregulated directly by RIN and indirectly through a lack of SREs.

RIN as a Direct and Indirect Potentiator of Gene Expression

Because the target mRNAs of RIN are enriched for GO terms related to multiple levels of the core gene expression machinery—transcription, splicing, and translation—RIN may directly potentiate the expression of its bound target transcripts and, in so doing, also indirectly upregulate gene expression globally. As an example of how RIN/G3BP's direct and indirect effects might converge on the same cellular process, we consider the production of cytoplasmic ribosomes. Metabolic labeling with

radioactive amino acids has shown that cytoplasmic ribosomal protein (cRP) synthesis increases after fertilization, peaks at 3–4 h, and subsequently decreases (Santon and Pellegrini, 1980, 1981). Recent ribosome occupancy-based measurements have confirmed that the translational efficiency of cRP mRNAs increases in early embryos relative to mature oocytes (Eichhorn et al., 2016). We have shown here that RIN potentiates target mRNA stability and translation and that cRP mRNAs are highly enriched among RIN's targets; thus, the potentiation of cRP mRNAs is expected to be a direct effect of RIN.

cRP mRNAs are also regulated by their conserved 5′-terminal oligopyrimidine (5′TOP) motifs (Meyuhas and Kahan, 2015). Two RBPs, La and Larp1, have been implicated in regulation of the stability and/or translation of 5′TOP mRNAs by this motif (Cardinali et al., 2003; Crosio et al., 2000; Fonseca et al., 2018; Pellizzoni et al., 1996; Tcherkezian et al., 2014). We have shown here that the *Drosophila* orthologs of both of these RBPs—LA and LARP—associate with RIN in an RNA-dependent manner. This could reflect the fact that LA, LARP, and RIN co-bind cRP mRNAs and, thus, that this class of mRNAs is subject to multiple direct mechanisms that potentiate its expression. Noteworthy is the fact that, of our RIN target mRNAs, only the cRP transcripts carry 5′TOP motifs and, as such, they represent a distinct class of mRNAs.

A possible indirect role of RIN in the regulation of cRP mRNAs relates to their upregulation by the Ragulator complex (Damgaard and Lykke-Andersen, 2011; Wilbertz et al., 2019). We have shown here that RIN binds mRNAs encoding all five subunits of the Ragulator complex. Thus, positive regulation by RIN of Ragulator subunit synthesis could indirectly promote cRP mRNA translation.

Direct and indirect regulation of other aspects of gene expression by RIN are also likely. Potentiation of production of core components of the transcription, splicing, and translation machinery might ensure that none of them becomes rate limiting for gene expression in rapidly developing early embryos. Likewise, adequate ATP production would be ensured by potentiation of expression of mitochondrial ribosomal proteins and components of the electron transport chain.

That said, our data suggest that the direct effects of RIN are much more pronounced than its indirect effects. Specifically, we have shown that, in *rin* mutants, levels of several target mRNAs are significantly reduced, whereas co-expressed non-targets do not change significantly. It should be noted, however, that these analyses were of a small subset of targets; future global analyses might reveal that indirect targets also change significantly.

A Function for RIN/G3BP Sequestration into SGs

Our data have implications for our understanding of how cells respond to stress and the role of SGs in that response. A theme in the cellular stress response is a general downregulation of mRNA expression. For example, stress triggers eukaryotic translation initiation factor 2 subunit alpha (eIF2α) phosphorylation, which prevents translation initiation (reviewed in Panas et al., 2016). This, in turn, triggers polysome disassembly, resulting in SG assembly. The storage of long mRNAs in SGs serves as a further mechanism to downregulate their translation. Based on our results, we propose that the recruitment of RIN/G3BPs into SGs would sequester these proteins from their short target mRNAs in the cytoplasm, serving to downregulate the expression of these transcripts. This could indirectly downregulate global gene expression by limiting the production of proteins involved in translation, transcription, and splicing. Likewise, if RIN/G3BPs serve to upregulate mitochondrial function and ATP production, sequestration could attenuate this aspect of cellular metabolism in stressed cells.

STAR★METHODS

Detailed methods are provided in the online version of this paper and include the following:

- KEY RESOURCES TABLE
- LEAD CONTACT AND MATERIALS AVAILABILITY
- EXPERIMENTAL MODEL AND SUBJECT DETAILS
- METHOD DETAILS
  - Western blots
  - Immunostaining of embryos
  - Generation of anti-RIN synthetic antibodies
  - Immunoprecipitations and mass spectrometry
  - Polysome gradients
  - RNA co-immunoprecipitations
  - Microarray analysis of RIN RIP samples
  - RT-qPCR
  - S2 cell transient transfection, dual-luciferase assay and RT-qPCR
  - S2 cell immunofluorescence and microscopy
- QUANTIFICATION AND STATISTICAL ANALYSIS
  - Mass spectrometry
  - Microarrays
  - Extraction of length-matched target and non-target sets
  - Enrichment test of published RIN motifs
  - Comparisons of RIN-associated mRNAs to published *Drosophila* datasets
  - Comparisons of RIN-associated mRNAs and proteins to datasets in other species
  - Gene ontology annotation enrichment analysis
- DATA AND CODE AVAILABILITY

SUPPLEMENTAL INFORMATION

Supplemental Information can be found online at https://doi.org/10.1016/j.celrep.2020.02.066.

ACKNOWLEDGMENTS

We thank the three anonymous reviewers for helpful feedback regarding the manuscript and the following for providing antibodies: Liz Gavis (anti-RIN) (Aguilera-Gomez et al., 2017) and Paul Macdonald (anti-CAPR) (Papoulas et al., 2010). The anti-FMR1 antibody (5A11) developed by H. Siomi was obtained from the Developmental Studies Hybridoma Bank, created by the National Institute of Child Health and Human Development (NICHD) of the National Institutes of Health (NIH), and maintained at the University of Iowa, Department of Biology, Iowa City, IA 52242. During the course of this research, we made extensive use of FlyBase and data from the Berkeley *Drosophila* Genome Project. This research was supported by Natural Sciences and

Engineering Research Council of Canada Discovery grants to H.D.L. (RGPIN-06246) and to C.A.S. (RGPIN-435985) and grants from the Canadian Institutes of Health Research to H.D.L. (PJT-159702) and Q.M. (MOP-125894).

AUTHOR CONTRIBUTIONS

Conceptualization: J.D.L., C.A.S., and H.D.L.; Methodology: J.D.L., C.A.S., H.D.L., S.A., Q.M., S.S.S., and J.T.W.; Investigation: J.D.L., J.L., A.K.W., S.L., A.K., G.B., W.X.C., N.J-L., and A.K.; Software and Formal Analysis: K.L., J.D.L., and Q.M.; Writing—Original Draft: J.D.L. and J.L.; Writing—Review and Editing: H.D.L. and C.A.S.; Funding Acquisition: H.D.L., C.A.S., and Q.M.; Resources: S.A., S.S.S., and J.T.W.; Supervision: C.A.S., H.D.L., S.A., and Q.M.

DECLARATION OF INTERESTS

The authors declare no competing interests.

Received: May 1, 2019
Revised: January 13, 2020
Accepted: February 14, 2020
Published: March 10, 2020

REFERENCES

Achsel, T., and Bagni, C. (2016). Cooperativity in RNA-protein interactions: the complex is more than the sum of its partners. Curr. Opin. Neurobiol. *39*, 146–151.

Adivarahan, S., Livingston, N., Nicholson, B., Rahman, S., Wu, B., Rissland, O.S., and Zenklusen, D. (2018). Spatial Organization of Single mRNPs at Different Stages of the Gene Expression Pathway. Mol. Cell *72*, 727–738.e725.

Aguilera-Gomez, A., Zacharogianni, M., van Oorschot, M.M., Genau, H., Grond, R., Veenendaal, T., Sinsimer, K.S., Gavis, E.A., Behrends, C., and Rabouille, C. (2017). Phospho-Rasputin Stabilization by Sec16 Is Required for Stress Granule Formation upon Amino Acid Starvation. Cell Rep. *20*, 2277.

Alam, U., and Kennedy, D. (2019). Rasputin a decade on and more promiscuous than ever? A review of G3BPs. Biochim. Biophys. Acta Mol. Cell Res. *1866*, 360–370.

Anderson, P., and Kedersha, N. (2009a). RNA granules: post-transcriptional and epigenetic modulators of gene expression. Nat. Rev. Mol. Cell Biol. *10*, 430–436.

Anderson, P., and Kedersha, N. (2009b). Stress granules. Curr. Biol. *19*, R397–R398.

Ashburner, M. (1989). Drosophila (Cold Spring Harbor Laboratory).

Aviv, T., Lin, Z., Lau, S., Rendl, L.M., Sicheri, F., and Smibert, C.A. (2003). The RNA-binding SAM domain of Smaug defines a new family of post-transcriptional regulators. Nat. Struct. Biol. *10*, 614–621.

Aviv, T., Lin, Z., Ben-Ari, G., Smibert, C.A., and Sicheri, F. (2006). Sequence-specific recognition of RNA hairpins by the SAM domain of Vts1p. Nat. Struct. Mol. Biol. *13*, 168–176.

Bar-Peled, L., Schweitzer, L.D., Zoncu, R., and Sabatini, D.M. (2012). Ragulator is a GEF for the rag GTPases that signal amino acid levels to mTORC1. Cell *150*, 1196–1208.

Baumgartner, R., Stocker, H., and Hafen, E. (2013). The RNA-binding proteins FMR1, rasputin and caprin act together with the UBA protein lingerer to restrict tissue growth in *Drosophila melanogaster*. PLoS Genet. *9*, e1003598.

Benoit, B., He, C.H., Zhang, F., Votruba, S.M., Tadros, W., Westwood, J.T., Smibert, C.A., Lipshitz, H.D., and Theurkauf, W.E. (2009). An essential role for the RNA-binding protein Smaug during the *Drosophila* maternal-to-zygotic transition. Development *136*, 923–932.

Bernhart, S.H., Hofacker, I.L., and Stadler, P.F. (2006). Local RNA base pairing probabilities in large sequences. Bioinformatics *22*, 614–615.

Bovaird, S., Patel, D., Padilla, J.A., and Lécuyer, E. (2018). Biological functions, regulatory mechanisms, and disease relevance of RNA localization pathways. FEBS Lett. *592*, 2948–2972.

Buchan, J.R., and Parker, R. (2009). Eukaryotic stress granules: the ins and outs of translation. Mol. Cell *36*, 932–941.

Bushati, N., Stark, A., Brennecke, J., and Cohen, S.M. (2008). Temporal reciprocity of miRNAs and their targets during the maternal-to-zygotic transition in *Drosophila*. Curr. Biol. *18*, 501–506.

Cardinali, B., Carissimi, C., Gravina, P., and Pierandrei-Amaldi, P. (2003). La protein is associated with terminal oligopyrimidine mRNAs in actively translating polysomes. J. Biol. Chem. *278*, 35145–35151.

Chen, L., Dumelie, J.G., Li, X., Cheng, M.H., Yang, Z., Laver, J.D., Siddiqui, N.U., Westwood, J.T., Morris, Q., Lipshitz, H.D., and Smibert, C.A. (2014). Global regulation of mRNA translation and stability in the early *Drosophila* embryo by the Smaug RNA-binding protein. Genome Biol. *15*, R4.

Chiu, C.W.N., Monat, C., Robitaille, M., Lacomme, M., Daulat, A.M., Macleod, G., McNeill, H., Cayouette, M., and Angers, S. (2016). SAPCD2 Controls Spindle Orientation and Asymmetric Divisions by Negatively Regulating the Gαi-LGN-NuMA Ternary Complex. Dev. Cell *36*, 50–62.

Choi, H., Larsen, B., Lin, Z.Y., Breitkreutz, A., Mellacheruvu, D., Fermin, D., Qin, Z.S., Tyers, M., Gingras, A.C., and Nesvizhskii, A.I. (2011). SAINT: probabilistic scoring of affinity purification-mass spectrometry data. Nat. Methods *8*, 70–73.

Cook, K.B., Kazan, H., Zuberi, K., Morris, Q., and Hughes, T.R. (2011). RBPDB: a database of RNA-binding specificities. Nucleic Acids Res. *39*, D301–D308.

Costa, A., Wang, Y., Dockendorff, T.C., Erdjument-Bromage, H., Tempst, P., Schedl, P., and Jongens, T.A. (2005). The *Drosophila* fragile X protein functions as a negative regulator in the orb autoregulatory pathway. Dev. Cell *8*, 331–342.

Costa, A., Pazman, C., Sinsimer, K.S., Wong, L.C., McLeod, I., Yates, J., III, Haynes, S., and Schedl, P. (2013). Rasputin functions as a positive regulator of orb in *Drosophila* oogenesis. PLoS One *8*, e72864.

Costello, J., Castelli, L.M., Rowe, W., Kershaw, C.J., Talavera, D., Mohammad-Qureshi, S.S., Sims, P.F., Grant, C.M., Pavitt, G.D., Hubbard, S.J., and Ashe, M.P. (2015). Global mRNA selection mechanisms for translation initiation. Genome Biol. *16*, 10.

Crosio, C., Boyl, P.P., Loreni, F., Pierandrei-Amaldi, P., and Amaldi, F. (2000). La protein has a positive effect on the translation of TOP mRNAs *in vivo*. Nucleic Acids Res. *28*, 2927–2934.

Damgaard, C.K., and Lykke-Andersen, J. (2011). Translational coregulation of 5'TOP mRNAs by TIA-1 and TIAR. Genes Dev. *25*, 2057–2068.

De Renzis, S., Elemento, O., Tavazoie, S., and Wieschaus, E.F. (2007). Unmasking activation of the zygotic genome using chromosomal deletions in the *Drosophila* embryo. PLoS Biol. *5*, e117.

Dunn, J.G., Foo, C.K., Belletier, N.G., Gavis, E.R., and Weissman, J.S. (2013). Ribosome profiling reveals pervasive and regulated stop codon readthrough in *Drosophila melanogaster*. eLife *2*, e01179.

Edupuganti, R.R., Geiger, S., Lindeboom, R.G.H., Shi, H., Hsu, P.J., Lu, Z., Wang, S.Y., Baltissen, M.P.A., Jansen, P.W.T.C., Rossa, M., et al. (2017). N^6-methyladenosine (m^6A) recruits and repels proteins to regulate mRNA homeostasis. Nat. Struct. Mol. Biol. *24*, 870–878.

Eichhorn, S.W., Subtelny, A.O., Kronja, I., Kwasnieski, J.C., Orr-Weaver, T.L., and Bartel, D.P. (2016). mRNA poly(A)-tail changes specified by deadenylation broadly reshape translation in *Drosophila* oocytes and early embryos. eLife *5*, e16955.

Fonseca, B.D., Lahr, R.M., Damgaard, C.K., Alain, T., and Berman, A.J. (2018). LARP1 on TOP of ribosome production. Wiley Interdiscip. Rev. RNA *2*, e1480.

Hafer, N., Xu, S., Bhat, K.M., and Schedl, P. (2011). The *Drosophila* CPEB protein Orb2 has a novel expression pattern and is important for asymmetric cell division and nervous system function. Genetics *189*, 907–921.

Harvey, R., Dezi, V., Pizzinga, M., and Willis, A.E. (2017). Post-transcriptional control of gene expression following stress: the role of RNA-binding proteins. Biochem. Soc. Trans. *45*, 1007–1014.

Hu, Y., Flockhart, I., Vinayagam, A., Bergwitz, C., Berger, B., Perrimon, N., and Mohr, S.E. (2011). An integrative approach to ortholog prediction for disease-focused and other functional studies. BMC Bioinformatics *12*, 357.

Huang, D.W., Sherman, B.T., and Lempicki, R.A. (2009a). Bioinformatics enrichment tools: paths toward the comprehensive functional analysis of large gene lists. Nucleic Acids Res. *37*, 1–13.

Huang, D.W., Sherman, B.T., Zheng, X., Yang, J., Imamichi, T., Stephens, R., and Lempicki, R.A. (2009b). Extracting biological meaning from large gene lists with DAVID. Curr. Protoc. Bioinformatics *Chapter 13*, Unit 13 11.

Iadevaia, V., and Gerber, A.P. (2015). Combinatorial Control of mRNA Fates by RNA-Binding Proteins and Non-Coding RNAs. Biomolecules *5*, 2207–2222.

Jain, S., Wheeler, J.R., Walters, R.W., Agrawal, A., Barsic, A., and Parker, R. (2016). ATPase-Modulated Stress Granules Contain a Diverse Proteome and Substructure. Cell *164*, 487–498.

Jiang, T., McKinley, R.F., McGill, M.A., Angers, S., and Harris, T.J. (2015). A Par-1-Par-3-Centrosome Cell Polarity Pathway and Its Tuning for Isotropic Cell Adhesion. Curr. Biol. *25*, 2701–2708.

Kan, L., Grozhik, A.V., Vedanayagam, J., Patil, D.P., Pang, N., Lim, K.S., Huang, Y.C., Joseph, B., Lin, C.J., Despic, V., et al. (2017). The m^6A pathway facilitates sex determination in *Drosophila*. Nat. Commun. *8*, 15737.

Kedersha, N., and Anderson, P. (2009). Regulation of translation by stress granules and processing bodies. Prog. Mol. Biol. Transl. Sci. *90*, 155–185.

Kedersha, N., Panas, M.D., Achorn, C.A., Lyons, S., Tisdale, S., Hickman, T., Thomas, M., Lieberman, J., McInerney, G.M., Ivanov, P., and Anderson, P. (2016). G3BP-Caprin1-USP10 complexes mediate stress granule condensation and associate with 40S subunits. J. Cell Biol. *212*, 845–860.

Khong, A., Matheny, T., Jain, S., Mitchell, S.F., Wheeler, J.R., and Parker, R. (2017). The Stress Granule Transcriptome Reveals Principles of mRNA Accumulation in Stress Granules. Mol. Cell *68*, 808–820.e805.

Knight, J.D.R., Choi, H., Gupta, G.D., Pelletier, L., Raught, B., Nesvizhskii, A.I., and Gingras, A.C. (2017). ProHits-viz: a suite of web tools for visualizing interaction proteomics data. Nat. Methods *14*, 645–646.

Kuhn, L., Majzoub, K., Einhorn, E., Chicher, J., Pompon, J., Imler, J.L., Hammann, P., and Meignin, C. (2017). Definition of a RACK1 Interaction Network in *Drosophila melanogaster* Using SWATH-MS. G3 (Bethesda) *7*, 2249–2258.

Laver, J.D., Ancevicius, K., Sollazzo, P., Westwood, J.T., Sidhu, S.S., Lipshitz, H.D., and Smibert, C.A. (2012). Synthetic antibodies as tools to probe RNA-binding protein function. Mol. Biosyst. *8*, 1650–1657.

Laver, J.D., Li, X., Ancevicius, K., Westwood, J.T., Smibert, C.A., Morris, Q.D., and Lipshitz, H.D. (2013). Genome-wide analysis of Staufen-associated mRNAs identifies secondary structures that confer target specificity. Nucleic Acids Res. *41*, 9438–9460.

Laver, J.D., Li, X., Ray, D., Cook, K.B., Hahn, N.A., Nabeel-Shah, S., Kekis, M., Luo, H., Marsolais, A.J., Fung, K.Y., et al. (2015a). Brain tumor is a sequence-specific RNA-binding protein that directs maternal mRNA clearance during the *Drosophila* maternal-to-zygotic transition. Genome Biol. *16*, 94.

Laver, J.D., Marsolais, A.J., Smibert, C.A., and Lipshitz, H.D. (2015b). Regulation and Function of Maternal Gene Products During the Maternal-to-Zygotic Transition in *Drosophila*. Curr. Top. Dev. Biol. *113*, 43–84.

Li, X., Quon, G., Lipshitz, H.D., and Morris, Q. (2010). Predicting *in vivo* binding sites of RNA-binding proteins using mRNA secondary structure. RNA *16*, 1096–1107.

Liu, G., Zhang, J., Larsen, B., Stark, C., Breitkreutz, A., Lin, Z.Y., Breitkreutz, B.J., Ding, Y., Colwill, K., Pasculescu, A., et al. (2010). ProHits: integrated software for mass spectrometry-based interaction proteomics. Nat. Biotechnol. *28*, 1015–1017.

Liu, Y.C., Couzens, A.L., Deshwar, A.R., B McBroom-Cerajewski, L.D., Zhang, X., Puviindran, V., Scott, I.C., Gingras, A.C., Hui, C.C., and Angers, S. (2014). The PPFIA1-PP2A protein complex promotes trafficking of Kif7 to the ciliary tip and Hedgehog signaling. Sci. Signal. *7*, ra117.

Lorenz, R., Bernhart, S.H., Höner Zu Siederdissen, C., Tafer, H., Flamm, C., Stadler, P.F., and Hofacker, I.L. (2011). ViennaRNA Package 2.0. Algorithms Mol. Biol. *6*, 26.

Luo, H., Li, X., Claycomb, J.M., and Lipshitz, H.D. (2016). The Smaug RNA-Binding Protein Is Essential for microRNA Synthesis During the *Drosophila* Maternal-to-Zygotic Transition. G3 (Bethesda) *6*, 3541–3551.

Markmiller, S., Soltanieh, S., Server, K.L., Mak, R., Jin, W., Fang, M.Y., Luo, E.C., Krach, F., Yang, D., Sen, A., et al. (2018). Context-Dependent and Disease-Specific Diversity in Protein Interactions within Stress Granules. Cell *172*, 590–604.e513.

Marygold, S.J., Roote, J., Reuter, G., Lambertsson, A., Ashburner, M., Millburn, G.H., Harrison, P.M., Yu, Z., Kenmochi, N., Kaufman, T.C., et al. (2007). The ribosomal protein genes and Minute loci of *Drosophila melanogaster*. Genome Biol. *8*, R216.

Meyuhas, O., and Kahan, T. (2015). The race to decipher the top secrets of TOP mRNAs. Biochim. Biophys. Acta *1849*, 801–811.

Mohan, R.D., Dialynas, G., Weake, V.M., Liu, J., Martin-Brown, S., Florens, L., Washburn, M.P., Workman, J.L., and Abmayr, S.M. (2014). Loss of *Drosophila* Ataxin-7, a SAGA subunit, reduces H2B ubiquitination and leads to neural and retinal degeneration. Genes Dev. *28*, 259–272.

Monzo, K., Papoulas, O., Cantin, G.T., Wang, Y., Yates, J.R., 3rd, and Sisson, J.C. (2006). Fragile X mental retardation protein controls trailer hitch expression and cleavage furrow formation in *Drosophila* embryos. Proc. Natl. Acad. Sci. USA *103*, 18160–18165.

Na, H., Laver, J.D., Jeon, J., Singh, F., Ancevicius, K., Fan, Y., Cao, W.X., Nie, K., Yang, Z., Luo, H., et al. (2016). A high-throughput pipeline for the production of synthetic antibodies for analysis of ribonucleoprotein complexes. RNA *22*, 636–655.

Namkoong, S., Ho, A., Woo, Y.M., Kwak, H., and Lee, J.H. (2018). Systematic Characterization of Stress-Induced RNA Granulation. Mol. Cell *70*, 175–187.e178.

Okamura, K., Ishizuka, A., Siomi, H., and Siomi, M.C. (2004). Distinct roles for Argonaute proteins in small RNA-directed RNA cleavage pathways. Genes Dev. *18*, 1655–1666.

Panas, M.D., Ivanov, P., and Anderson, P. (2016). Mechanistic insights into mammalian stress granule dynamics. J. Cell Biol. *215*, 313–323.

Papoulas, O., Monzo, K.F., Cantin, G.T., Ruse, C., Yates, J.R., 3rd, Ryu, Y.H., and Sisson, J.C. (2010). dFMRP and Caprin, translational regulators of synaptic plasticity, control the cell cycle at the *Drosophila* mid-blastula transition. Development *137*, 4201–4209.

Pazman, C., Mayes, C.A., Fanto, M., Haynes, S.R., and Mlodzik, M. (2000). Rasputin, the *Drosophila* homologue of the RasGAP SH3 binding protein, functions in ras- and Rho-mediated signaling. Development *127*, 1715–1725.

Pellizzoni, L., Cardinali, B., Lin-Marq, N., Mercanti, D., and Pierandrei-Amaldi, P. (1996). A *Xenopus laevis* homologue of the La autoantigen binds the pyrimidine tract of the 5′ UTR of ribosomal protein mRNAs *in vitro*: implication of a protein factor in complex formation. J. Mol. Biol. *259*, 904–915.

Persson, H., Ye, W., Wernimont, A., Adams, J.J., Koide, A., Koide, S., Lam, R., and Sidhu, S.S. (2013). CDR-H3 diversity is not required for antigen recognition by synthetic antibodies. J. Mol. Biol. *425*, 803–811.

Pinder, B.D., and Smibert, C.A. (2013). microRNA-independent recruitment of Argonaute 1 to nanos mRNA through the Smaug RNA-binding protein. EMBO Rep. *14*, 80–86.

Protter, D.S.W., and Parker, R. (2016). Principles and Properties of Stress Granules. Trends Cell Biol. *26*, 668–679.

Ray, D., Kazan, H., Cook, K.B., Weirauch, M.T., Najafabadi, H.S., Li, X., Guerroussov, S., Albu, M., Zheng, H., Yang, A., et al. (2013). A compendium of RNA-binding motifs for decoding gene regulation. Nature *499*, 172–177.

Saeed, A.I., Sharov, V., White, J., Li, J., Liang, W., Bhagabati, N., Braisted, J., Klapa, M., Currier, T., Thiagarajan, M., et al. (2003). TM4: a free, open-source system for microarray data management and analysis. Biotechniques *34*, 374–378.

Saeed, A.I., Bhagabati, N.K., Braisted, J.C., Liang, W., Sharov, V., Howe, E.A., Li, J., Thiagarajan, M., White, J.A., and Quackenbush, J. (2006). TM4 microarray software suite. Methods Enzymol. *411*, 134–193.

Sancak, Y., Bar-Peled, L., Zoncu, R., Markhard, A.L., Nada, S., and Sabatini, D.M. (2010). Ragulator-Rag complex targets mTORC1 to the lysosomal surface and is necessary for its activation by amino acids. Cell *141*, 290–303.

Santon, J.B., and Pellegrini, M. (1980). Expression of ribosomal proteins during *Drosophila* early development. Proc. Natl. Acad. Sci. USA *77*, 5649–5653.

Santon, J.B., and Pellegrini, M. (1981). Rates of ribosomal protein and total protein synthesis during *Drosophila* early embryogenesis. Dev. Biol. *85*, 252–257.

Schindelin, J., Arganda-Carreras, I., Frise, E., Kaynig, V., Longair, M., Pietzsch, T., Preibisch, S., Rueden, C., Saalfeld, S., Schmid, B., et al. (2012). Fiji: an open-source platform for biological-image analysis. Nat. Methods *9*, 676–682.

Schneider, C.A., Rasband, W.S., and Eliceiri, K.W. (2012). NIH Image to ImageJ: 25 years of image analysis. Nat. Methods *9*, 671–675.

Semotok, J.L., Cooperstock, R.L., Pinder, B.D., Vari, H.K., Lipshitz, H.D., and Smibert, C.A. (2005). Smaug recruits the CCR4/POP2/NOT deadenylase complex to trigger maternal transcript localization in the early *Drosophila* embryo. Curr. Biol. *15*, 284–294.

Semotok, J.L., Luo, H., Cooperstock, R.L., Karaiskakis, A., Vari, H.K., Smibert, C.A., and Lipshitz, H.D. (2008). *Drosophila* maternal Hsp83 mRNA destabilization is directed by multiple SMAUG recognition elements in the open reading frame. Mol. Cell. Biol. *28*, 6757–6772.

Smibert, C.A., Wilson, J.E., Kerr, K., and Macdonald, P.M. (1996). smaug protein represses translation of unlocalized *nanos* mRNA in the *Drosophila* embryo. Genes Dev. *10*, 2600–2609.

Smibert, C.A., Lie, Y.S., Shillinglaw, W., Henzel, W.J., and Macdonald, P.M. (1999). Smaug, a novel and conserved protein, contributes to repression of nanos mRNA translation *in vitro*. RNA *5*, 1535–1547.

Solomon, S., Xu, Y., Wang, B., David, M.D., Schubert, P., Kennedy, D., and Schrader, J.W. (2007). Distinct structural features of caprin-1 mediate its interaction with G3BP-1 and its induction of phosphorylation of eukaryotic translation initiation factor 2alpha, entry to cytoplasmic stress granules, and selective interaction with a subset of mRNAs. Mol. Cell. Biol. *27*, 2324–2342.

Tadros, W., and Lipshitz, H.D. (2009). The maternal-to-zygotic transition: a play in two acts. Development *136*, 3033–3042.

Tadros, W., Goldman, A.L., Babak, T., Menzies, F., Vardy, L., Orr-Weaver, T., Hughes, T.R., Westwood, J.T., Smibert, C.A., and Lipshitz, H.D. (2007). SMAUG is a major regulator of maternal mRNA destabilization in *Drosophila* and its translation is activated by the PAN GU kinase. Dev. Cell *12*, 143–155.

Tareen, A., and Kinney, J.B. (2019). Logomaker: beautiful sequence logos in Python. Bioinformatics, btz921.

Tcherkezian, J., Cargnello, M., Romeo, Y., Huttlin, E.L., Lavoie, G., Gygi, S.P., and Roux, P.P. (2014). Proteomic analysis of cap-dependent translation identifies LARP1 as a key regulator of 5'TOP mRNA translation. Genes Dev. *28*, 357–371.

Thompson, M.K., and Gilbert, W.V. (2017). mRNA length-sensing in eukaryotic translation: reconsidering the "closed loop" and its implications for translational control. Curr. Genet. *63*, 613–620.

Thompson, M.K., Rojas-Duran, M.F., Gangaramani, P., and Gilbert, W.V. (2016). The ribosomal protein Asc1/RACK1 is required for efficient translation of short mRNAs. eLife *5*, e11154.

Thomsen, S., Anders, S., Janga, S.C., Huber, W., and Alonso, C.R. (2010). Genome-wide analysis of mRNA decay patterns during early *Drosophila* development. Genome Biol. *11*, R93.

Tourrière, H., Chebli, K., Zekri, L., Courselaud, B., Blanchard, J.M., Bertrand, E., and Tazi, J. (2003). The RasGAP-associated endoribonuclease G3BP assembles stress granules. J. Cell Biol. *160*, 823–831.

Tusher, V.G., Tibshirani, R., and Chu, G. (2001). Significance analysis of microarrays applied to the ionizing radiation response. Proc. Natl. Acad. Sci. USA *98*, 5116–5121.

Tutucci, E., Livingston, N.M., Singer, R.H., and Wu, B. (2018). Imaging mRNA *In Vivo*, from Birth to Death. Annu. Rev. Biophys. *47*, 85–106.

Van Treeck, B., and Parker, R. (2018). Emerging Roles for Intermolecular RNA-RNA Interactions in RNP Assemblies. Cell *174*, 791–802.

Vastenhouw, N.L., Cao, W.X., and Lipshitz, H.D. (2019). The maternal-to-zygotic transition revisited. Development *146*, dev161471.

Wagih, O. (2017). ggseqlogo: a versatile R package for drawing sequence logos. Bioinformatics *33*, 3645–3647.

Wakiyama, M., Kaitsu, Y., Muramatsu, R., Takimoto, K., and Yokoyama, S. (2012). Tethering of proteins to RNAs using the bovine immunodeficiency virus-Tat peptide and BIV-TAR RNA. Anal. Biochem. *427*, 130–132.

Wilbertz, J.H., Voigt, F., Horvathova, I., Roth, G., Zhan, Y., and Chao, J.A. (2019). Single-Molecule Imaging of mRNA Localization and Regulation during the Integrated Stress Response. Mol. Cell *73*, 946–958.e947.

Youn, J.Y., Dunham, W.H., Hong, S.J., Knight, J.D.R., Bashkurov, M., Chen, G.I., Bagci, H., Rathod, B., MacLeod, G., Eng, S.W.M., et al. (2018). High-Density Proximity Mapping Reveals the Subcellular Organization of mRNA-Associated Granules and Bodies. Mol. Cell *69*, 517–532.e511.

STAR★METHODS

KEY RESOURCES TABLE

REAGENT or RESOURCE	SOURCE	IDENTIFIER
Antibodies		
α-RIN D072 synthetic antigen-binding fragment (Fab)	This paper	N/A
α-RIN D074 synthetic antigen-binding fragment (Fab)	This paper	N/A
α-CAPR rabbit polyclonal	Paul Macdonald	Papoulas et al., 2010; RRID: AB_2569117
α-RIN rabbit polyclonal	Liz Gavis	Aguilera-Gomez et al., 2017
α-FMR1 mouse monoclonal 5A11	Developmental Studies Hybridoma Bank	Okamura et al., 2004; RRID: AB_528252
α-alpha-tubulin mouse monoclonal B-5-1-2	Sigma-Aldrich	Cat#T5168; RRID: AB_477579
α-FLAG mouse monoclonal M2	Sigma-Aldrich	Cat#F3165; RRID: AB_259529
α-FLAG M2 affinity agarose beads	Sigma-Aldrich	Cat#A2220; RRID: AB_10063035
α-mouse Alexa Flour 555	Invitrogen	Cat#A21424; RRID: AB_141780
α-rabbit Alexa Fluor 488	Invitrogen	Cat#A11034; RRID: AB_2576217
α-mouse Alexa Fluor 488	Invitrogen	Cat#A11029; RRID: AB_138404
α-rabbit Alexa Fluor 555	Invitrogen	Cat#A21429; RRID: AB_141761
Peroxidase-AffiniPure Goat α-Mouse IgG (H+L)	Jackson Immunoresearch Labs	Cat#115-035-003; RRID: AB_10015289
Peroxidase-AffiniPure Goat α-Rabbit IgG (H+L)	Jackson Immunoresearch Labs	Cat#111-035-144; RRID: AB_2307391
Chemicals, Peptides, and Recombinant Proteins		
Fluoromount g + DAPI	Invitrogen	Cat#00-4959-52
Poly-D-lysine hydrobromide	Sigma-Aldrich	Cat#P7886
DAPI	Sigma-Aldrich	Cat#D9542
Trizol Reagent	Invitrogen	Cat#15596018
Superscript IV Reverse Transcriptase	Invitrogen	Cat#18090050
dNTP Mix	Thermo Scientific	Cat#R0192
RNaseOUT Recombinant Ribonuclease Inhibitor	Invitrogen	Cat#10777019
Ultrapure water	Invitrogen	Cat#10977015
AEBSF	Bioshop	Cat#AEB602
Benzamidine	Bioshop	Cat#BEN666
Pepstatin	Bioshop	Cat#PEP605
Leupeptin	Bioshop	Cat#LEU001
DTT	Bioshop	Cat#DDT001
Triton X-100	BioShop	Cat#TRX777
Bio-Rad Protein Assay Dye Reagent	Bio-Rad	Cat#5000006
30% Acrylamide/Bis-acrylamide solution (37.5:1)	Bio-Rad	Cat#1610158
Skim Milk powder	BioShop	Cat#SKI400
Immuno-Blot PVDF	Bio-Rad	Cat#1620177
Puromycin	Bioshop	Cat#PUR333
Cycloheximide	Bioshop	Cat#CYC003
RiboLock RNase Inhibitor	Thermo Scientific	Cat# EO0381
Critical Commercial Assays		
SensiFAST SYBR No-ROX Kit	BioLine Meridian Bioscience	Cat#BIO-98050
Dual Luciferase Kit	Promega	Cat#E1910
Millipore Immobilon Luminata Crescendo Western HRP Substrate	Sigma-Aldrich	Cat#WBLUR0500
Deposited Data		
RIN (α-RIN D072) RIP-Chip raw and analyzed data	This paper	GEO: GSE12900
Flybase *Drosophila melanogaster* sequences v6.20	FlyBase Consortium	ftp://ftp.flybase.net/releases/FB2018_01/dmel_r6.20/fasta/

(*Continued on next page*)

Continued

REAGENT or RESOURCE	SOURCE	IDENTIFIER
Drosophila oogenesis and embryogenesis mRNA abundance and mRNA translational efficiency data	Eichhorn et al., 2016	N/A
Drosophila embryo mRNA translational efficiency data	Dunn et al., 2013	N/A
Drosophila embryo N6-methyladenosine mRNA modification data	Edupuganti et al., 2017	N/A
Drosophila early embryo mRNA stability, decay, and transcription transcript classes	Thomsen et al., 2010	N/A
Drosophila unfertilized egg unstable mRNA dataset	Tadros et al., 2007	N/A
Drosophila early embryo unstable mRNA dataset	De Renzis et al., 2007	N/A
Drosophila ribosomal protein gene lists	Marygold et al., 2007	N/A
Drosophila ovary RIN protein interaction data	Costa et al., 2013	N/A
Yeast and human stress granule proteome datasets	Jain et al., 2016	N/A
HEK293 and human neural progenitor cell stress granule proteome datasets	Markmiller et al., 2018	N/A
Human G3BP1-interacting proteins and human "core" stress granule and P-body proteome datasets	Youn et al., 2018	N/A
Human U2OS cell stress granule enrichment and depletion datasets	Khong et al., 2017	N/A
NIH 3T3 cell stress-induced insoluble RNA granule transcriptome datasets	Namkoong et al., 2018	N/A
Experimental Models: Cell Lines		
D. melanogaster Cell line S2	Drosophila Genomics Resource Center	Stock #181
Experimental Models: Organisms/Strains		
w^{1118}	Bloomington Drosophila Stock Centre	Stock #3605
w^{1118}; rin^{2}/TM6B, Sb^{1}	Bloomington Drosophila Stock Centre	Stock #9303
w^{1118}; rin^{3}/TM6B, Sb^{1} Tb^{1}	Bloomington Drosophila Stock Centre	Stock #57694
Oligonucleotides		
Random Hexamer Primer	Thermo Scientific	Cat#SO142
Anchored Oligo$(dT)_{20}$ Primer	Invitrogen	Cat#12577011
Primers used for RT-qPCR experiments: see Table S7	This paper	N/A
Recombinant DNA		
Plasmid: pRm-Rluc - expresses the Renilla luciferase ORF under the control of the metallothionein promoter	This paper	C2009
Plasmid: pRm-Fluc6xTAR - expresses the Firefly luciferase ORF under the control of the metallothionein promoter with 6 TAR stem/loops in the reporters 3′UTR	This paper	NJ2
Plasmid: pTat-FLAG-rin - the rin ORF under the control of the Actin5C promoter carrying an amino terminal Tat peptide and 3 FLAG tags	This paper	JY33
Plasmid: pTat-FLAG-G3BP1 - the G3BP1 ORF under the control of the Actin5C promoter carrying an amino terminal Tat peptide and 3 FLAG tags	This paper	JY125
Plasmid: pTat-FLAG-G3BP2 - the G3BP2 ORF under the control of the Actin5C promoter carrying an amino terminal Tat peptide and 3 FLAG tags	This paper	JY126
Plasmid: pTat-FLAG-GFP - the GFP ORF under the control of the Actin5C promoter carrying an amino terminal Tat peptide and 3 FLAG tags	This paper	AW14
Plasmid: pFLAG-GST - the GST ORF under the control of the Actin5C promoter carrying 3 amino terminal FLAG tags	This paper	JY110
Plasmid: D072 - encodes anti-RIN FAB	This paper	D072

(*Continued on next page*)

Continued

REAGENT or RESOURCE	SOURCE	IDENTIFIER
Plasmid: D074 - encodes anti-RIN FAB	This paper	D074
Software and Algorithms		
ProHits software package	Liu et al., 2010	http://prohitsms.comProhits_download/list.php
MultiExperiment Viewer	Saeed et al., 2006	http://mev.tm4.org
DAVID 6.8 functional annotation tool web server	Huang et al., 2009a, 2009b	https://david.ncifcrf.gov/
DRSC Integrative Ortholog Prediction Tool (DIOPT)	Hu et al., 2011	https://www.flyrnai.org/diopt
ImageJ	Schneider et al., 2012	https://imagej.nih.gov/ij/
Fiji	Schindelin et al., 2012	https://imagej.net/Fiji
RNAplfold (v2.4.6)	Lorenz et al., 2011	https://www.tbi.univie.ac.at/RNA/
ggseqlogo	Wagih, 2017	https://github.com/omarwagih/ggseqlogo
Logomaker	Tareen and Kinney, 2019	https://github.com/jbkinney/logomaker
Other		
Human G3BP1, G3BP2 *in vivo* binding motifs	Edupuganti et al., 2017	https://www.nature.com/articles/nsmb.3462
Human G3BP2, Drosophila RIN *in vitro* binding motifs	Ray et al., 2013	http://cisbp-rna.ccbr.utoronto.ca/
Synthetic antigen-binding fragment (Fab) Library F	Persson et al., 2013	N/A
SuperScript IV Reverse Transcriptase	Invitrogen	Cat#18090050
Custom-designed *Drosophila* 4x72K microarray	Roche NimbleGen	GEO: GPL10539

LEAD CONTACT AND MATERIALS AVAILABILITY

Further information and requests for resources and reagents should be directed to and will be fulfilled by the Lead Contact, Howard Lipshitz (howard.lipshitz@utoronto.ca). All unique/stable reagents generated in this study are available to researchers from the Lead Contact without restriction.

EXPERIMENTAL MODEL AND SUBJECT DETAILS

Wild-type *Drosophila* stock was w^{1118}; mutant lines were rin^{2}/*TM6B, Sb* (BDSC# 9303) (Pazman et al., 2000), and rin^{3}/*TM6B, Sb Tb* (BDSC# 57694) (Costa et al., 2013). The latter two lines were crossed to produce rin^{2}/rin^{3} mutants for RT-qPCR analysis. *Drosophila* S2 tissue culture cells were maintained at 25°C in Express Five SFM (Fisher Scientific) containing 100units/mL penicillin, 100μg /mL streptomycin and 16mM glutamine.

METHOD DETAILS

Western blots

Embryos were collected from cages containing w^{1118} flies, dechorionated with 100% bleach for 2 min, washed with 0.1% Triton X-100 and lysed by crushing in a minimal volume of lysis buffer: 150 mM KCl, 20 mM HEPES-KOH pH 7.4, 1 mM $MgCl_2$, supplemented with protease inhibitors (1 mM AEBSF, 2 mM benzamidine, 2 μg/mL pepstatin, 2 μg/mL leupeptin) and 1 mM DTT. The lysate was cleared by centrifugation (15 min at 4°C, 13000 RPM) and stored at –80°C. Protein concentration was determined using the Bio-Rad Protein Assay Dye Reagent (Cat#5000006) and 15μg total protein was resolved by SDS-PAGE. For S2 cell western blots, $1.2x10^{6}$ cells were pelleted via centrifugation and lysed with 2xSDS sample buffer supplemented with 1 mM AEBSF and boiling for 3 m. Two to eight μL of the resulting extracts were resolved via SDS-PAGE. Proteins were transferred to PVDF membrane, blocked at room temperature for 1 h with 0.5% milk in PBST (1x PBS + 0.1% Triton X-100). Blots were then incubated with the appropriate antibodies: anti-RIN (1:50000) (Aguilera-Gomez et al., 2017) and anti-α tubulin (1:10000, Sigma-Aldrich T5168), or anti-FLAG (1 μg/mL, Sigma-Aldrich F3165) at 4°C overnight. After incubation with primary antibody, the blot was incubated with HRP-conjugated secondary antibody (1:5000; either of Peroxidase-Affinipure goat α-mouse IgG (H+L) Cat#115-035-003 or goat α-rabbit IgG (H+L) Cat#115-035-144, Jackson Immunoresearch) at room temperature for 1 h. Western blots were developed using the ECL detection system (Millipore Immobilon Luminata Crescendo Western HRP substrate Cat#WBLUR0500). Relative levels of RIN and α-tubulin were determined using a standard curve. Western blots were imaged and quantified using ImageLab (BioRad).

Immunostaining of embryos

Standard immunostaining procedures were followed (Ashburner, 1989). Embryos were collected after a 4 h egg-lay from cages containing either w^{1118}, rin^{2}/rin^{3} mutant females or females heterozygous for *rin*. Embryos were dechorionated with 50% bleach and fixed in formaldehyde (4%) and methanol. To visualize RIN and FMR1, fixed embryos were incubated with the following primary antibodies used at the concentrations indicated: rabbit anti-RIN (1:1000; provided by Liz Gavis) (Aguilera-Gomez et al., 2017) and mouse anti-FMR1 (1:10; #5A11 from the Developmental Studies Hybridoma Bank) (Okamura et al., 2004). Conjugated secondary antibodies were purchased from Invitrogen-ThermoFisher and used at 1:300 (Alexa Fluor555 Goat Anti-Rabbit IgG, Catalog number A21429, and Alexa Fluor488 Goat Anti-Mouse IgG, Catalog number A11029). Embryos were also labeled for DNA using a 0.001mg/ml DAPI (Sigma, Catalog number D9542) incubation for 10 min. Images were collected using a Nikon Ti-S inverted microscope with Nikon C2 confocal system, using NIS Elements AR software. Images were then processed for figures using Fiji/ImageJ (Schindelin et al., 2012; Schneider et al., 2012), Adobe Photoshop and Adobe Illustrator.

Generation of anti-RIN synthetic antibodies

Synthetic antibodies were generated against antigens comprising RIN amino acids 12-131 (antibody D072) or amino acids 12-170 (antibody D074; all amino acid numbering according to RIN-PB isoform), which were expressed and purified from *E. coli* as GST fusion proteins as described (Laver et al., 2012). Synthetic antibodies were obtained by performing five rounds of binding selection with synthetic antibody Library F (Persson et al., 2013) against each of the two RIN antigens, as described (Laver et al., 2015a). The synthetic antibodies obtained against RIN were expressed and purified from *E. coli* as Fabs, tagged at the C terminus of the light chain with a FLAG tag, as described (Laver et al., 2012).

Immunoprecipitations and mass spectrometry

For RIN IP-MS experiments, 0–3 h old embryos were collected, and lysed by crushing in a minimal volume of lysis buffer (150 mM KCl, 20 mM HEPES-KOH pH 7.4, 1 mM $MgCl_2$, supplemented with protease inhibitors and 1 mM DTT), followed with clearing by centrifugation (15 min at 4°C; 20,000 x g), and stored at –80°C. Immediately prior to performing IPs, this cleared lysate was thawed and diluted 1/2 with lysis buffer, and supplemented with Triton X-100 to a final concentration of 0.1%. For IPs, ~800 μL of this diluted lysate, with or without 0.35 μg/μL RNase A, was incubated with 40 μL of anti-FLAG M2 beads (Sigma) that were pre-loaded with 20 μg of either RIN Fab D072 or control C1 Fab, and blocked with BSA. IPs were incubated for ~3 h at 4°C with end-over-end rotation. After incubation, beads were washed 4–5 times with lysis buffer supplemented with 0.1% Triton X-100, twice with lysis buffer (no Triton X-100), then transferred to new tubes and washed twice with lysis buffer (no Triton X-100). Bound proteins were eluted by tryptic digest: beads were resuspended in 200 μL of 50 mM ammonium bicarbonate pH 8, supplemented with 2 μg of trypsin, and incubated overnight at room temperature with end-over-end rotation. The following day, the digested supernatant was recovered, and beads were washed once with an additional 200 μL of 50 mM ammonium bicarbonate to collect any residual eluted material. The two supernatants were pooled and dried by speed-vac. Liquid chromatography–tandem mass spectrometry (LC-MS/MS) was performed using the Thermo Q-Exactive HF quadrupole-Orbitrap mass spectrometer (Thermo Scientific) and the methods followed those previously described (Chiu et al., 2016; Jiang et al., 2015; Liu et al., 2014).

Three biological replicates of RIN IPs and control IPs were performed, in both the presence and absence of RNase A. Data analysis is described below.

Polysome gradients

Embryos were collected 0–3 h post egg laying and lysed in a 2 mLs of lysis buffer per gram of embryos. Lysis buffer was 50 mM Tris pH 7.5, 2mM $MgCl_2$, 150 mM KCl, 100 μM GTP, 1 mM DTT, 50 U/mL RNase inhibitor, 1 mM AEBSF, 2 μg/mL leupeptin, 2 mM benzamidine, 2 μg/mL pepstatin A that was supplemented with either 0.5 mg/mL cycloheximide or 2mM puromycin. After lysis samples were left on ice for 20 min and then incubated at 30°C for 10 min. 30% Triton X-100 was added to a final concentration of 1% and samples were spun at 6000 x g for 10 min. 400 μL the resulting supernatant was layered onto a 5mL 15% to 45% sucrose gradient in 7.5 mM $MgCl_2$, 500 mM NaCl, and 50 mM Tris pH 7.5. The gradient was created using a BioComp Model 117 Gradient Mate gradient maker (BioComp) using according to the manufacter's instructions. The gradients were chilled on ice for 1 h before extract application after which they were spin at 36,000 rpm for 2h 30 min at 4°C in a Beckman SW50.1 rotor. The gradients were then hand fractionated into nine 600 μL fractions which were analyzed via western blot.

RNA co-immunoprecipitations

For RNA co-immunoprecipitations for RIP-Chip experiments, immunoprecipitations were carried out from 400 μL of embryo lysate, prepared from embryos collected 0–3 h post-egg-laying, using 20 μg of FLAG-tagged Fab captured on 40 μL of anti-FLAG M2 affinity gel (Sigma), as previously described (Laver et al., 2015a). RNA co-immunoprecipitations for RT-qPCR experiments were performed similarly but at a reduced scale, using one-eighth the amount of material listed above.

Microarray analysis of RIN RIP samples

Microarrays were custom-designed *Drosophila* 4 × 72 K NimbleGen arrays (GEO platform number: GPL10539). RIP samples were reverse-transcribed, labeled, and hybridized as previously described (Laver et al., 2015a). Three biological replicates each

were performed for RIN and control immunoprecipitated samples. Arrays were scanned, quantified, and normalized as previously described (Laver et al., 2015a), with all RIN and control IP samples normalized together. The data have been deposited in the Gene Expression Omnibus (GEO) under accession number GEO: GSE12900. Analysis is described below.

RT-qPCR

For RT-qPCR from RIN RNA co-immunoprecipitations, single-stranded cDNA was synthesized by reverse transcription of immunoprecipitated RNA with Superscript IV reverse transcriptase (Invitrogen) using a mixture of random hexamer and anchored oligo-dT primers, as described for cDNA synthesis for microarray sample preparation (Laver et al., 2015a). The single-stranded cDNA was used to perform quantitative real-time PCR with primers specific to the various transcripts assayed, using SensiFAST SYBR PCR mix (Bioline) and a CFX384 Real-Time System (Bio-Rad). Sequences of the primers used for PCR are listed in Table S7.

S2 cell transient transfection, dual-luciferase assay and RT-qPCR

Drosophila S2 tissue culture cells were maintained at 25°C in Express Five SFM (Fisher Scientific) containing 100units/mL penicillin, 100μg/mL streptomycin and 16mM glutamine. A mixture of 1.5ng Firefly luciferase-6x TAR plasmid, 1.5ng *Renilla* luciferase plasmid, 3ng Tat-FLAG-effector plasmid (carrying either the GFP, RIN, G3BP1 or G3BP2 open reading frame), 1.5ng of FLAG-GST and 192.5ng pSP72 was transfected into 0.4mL of S2 cells at a density of 1.75×10^6 cells/mL using 0.4 μL TransIT-Insect transfection reagent (Mirus Bio), according to the manufacturer's instructions. Both luciferase reporters were cloned into pRmHa3 (Mohan et al., 2014) and, thus, were under the control of the metal-inducible metallothionein promoter. All FLAG-tagged constructs were derived from pAc5.1/V5-His (Thermo Fisher Scientific), which carries the Actin5C promoter. The expression of luciferase reporters was induced 24 h post transfection through the addition of copper sulfate to a final concentration of 0.5mM. 24 h post induction, Firefly and *Renilla* luciferase activities were measured using the Dual-Luciferase Reporter Assay System (Promega). In indicated experiments, the amount of transfected Tat-GFP was reduced to 0.3ng and 2.7ng of a pAc5.1/V5-His derivative expressing only Tat-FLAG was included to maintain equal levels of actin promoter across all transfections.

To assay reporter transcript levels, 48 h post-transfection S2 cells were harvested, resuspended in TRI reagent (MRC) and RNA was purified according to the manufacturer's protocol. 1ug of total RNA was treated with DNase I (Invitrogen) after which it was used to generate cDNA through reverse transcription with Superscript IV reverse transcriptase (Invitrogen) and random hexamers (Thermo Fisher) following the manufacturer's instructions. The cDNA was subjected to quantitative real-time PCR using the SensiFAST SYBR PCR mix (Bioline) PCR mix and primers against the Firefly and *Renilla* luciferase ORFs. Relative levels of the Firefly and *Renilla* transcripts were determined using a standard curve. Sequences of the primers used for PCR are listed in Table S7.

S2 cell immunofluorescence and microscopy

Forty-eight h post-transfection S2 cells were grown at 25°C on poly-D-lysine coated coverslips for 3 h. Following any treatment, cells were immediately fixed with 4% EM grade formaldehyde in PBS for 10 min. Cells were rinsed once with PBSTx (1X PBS+0.1% Triton X-100), permeablized with PBSTx for 15 min then incubated with 5μg/mL α-FLAG M2 (F3165, Sigma) and 1:200 rabbit α-CAPR (Papoulas et al., 2010) overnight at 4C in a humidified chamber. Coverslips were washed 3 times for 5 min each time with PBSTx then incubated with α-mouse Alexa Flour 555 and α-rabbit Alexa Fluor 488 (Invitrogen-ThermoFisher Catalog numbers A21424 and A11034, respectively) for 2 h at room temp in a humidified chamber. Coverslips were washed 3 times for 5 min each with PSBTx and then mounted onto slides with Fluoromount g + DAPI (00-4959-52, Invitrogen) and incubated overnight at 4°C. All images were collected using a Nikon Ti-S confocal microscope with NIS Elements AR software. Images were processed using ImageJ.

QUANTIFICATION AND STATISTICAL ANALYSIS

Mass spectrometry

To identify RIN-interacting proteins, we used the ProHits software package (Liu et al., 2010) to perform Significance Analysis of INTeractome (SAINT), comparing RNase-treated RIN IP versus control IP samples, and non-RNase-treated RIN IP versus control IP samples. Specifically, SAINT input files were generated using the "TPP iProphet" search engine option in ProHits, filtering for iProphet probability >0.95 and number of unique peptides < 2. SAINTexpress (exp3.3) was run using the ProHits interface, including only detected *Drosophila* proteins, with the following settings: number of compressed controls = 3; burn-in period, nburn = 2000; iterations, niter = 5000; lowMode = 1; minFold = 1; normalize = 1; nCompressBaits = 2. Identified proteins were defined as RNA-independent or RNA-dependent RIN-interacting proteins, if, in the analyses of the respective samples, they achieved a SAINT score $\geq$ 0.95 and a Bayesian false discovery rate (BFDR) $\leq$ 0.01.

Microarrays

To identify RIN-associated mRNAs, microarray data were analyzed using the Significance Analysis of Microarrays (SAM) (Tusher et al., 2001) function available in the MultiExperiment Viewer software application (Saeed et al., 2006; Saeed et al., 2003), as previously described (Laver et al., 2015a). Genes whose mRNAs were significantly enriched in the anti-RIN IPs compared to the control IPs, with an FDR of less than 5% and at least two-fold enrichment, were defined as RIN-associated mRNAs.

For the purposes of all subsequent analyses, FBgn gene IDs listed in the array annotation file were updated to FlyBase release 6.20 using the 'Upload/Convert IDs' tool available on FlyBase, and mRNAs corresponding to gene models which have since been withdrawn were excluded.

Extraction of length-matched target and non-target sets

Length-matched targets and non-targets were extracted as follows: first, we randomly chose a target transcript from the target set, and then we looked for a transcript in the non-target set that had the minimum length difference from that target, unless the length differences for the remaining non-targets were all higher or equal to the length of the target transcript (we randomly chose one if multiple non-targets with the same length difference were available). Non-targets were removed from the candidate non-target set when they were selected as a match for a target, and targets were removed from the candidate target set whether or not they had a match in the non-target set. We repeated this process until we exhausted the target set. Because RIN targets are generally shorter than non-targets, and the order of RIN targets being chosen from the target set was different for each matching process, the composition of the length-matched target and non-target sets was different in each iteration (five such iterations were carried out; see Tables S3 and S4). We extracted multiple length-matched target and non-target sets for 5′UTR, CDS, 3′UTR and full mRNA, using the sequence length of each transcriptomic region respectively.

Enrichment test of published RIN motifs

To test whether published RIN motifs are enriched in genes co-immunoprecipitated with RIN in our analysis, we used *in vitro*-determined *Drosophila* RIN and human G3BP2 motifs (Cook et al., 2011; Ray et al., 2013) (see http://cisbp-rna.ccbr.utoronto.ca/), and *in vivo* motifs of human G3BP1 and G3BP2 (Edupuganti et al., 2017). Position frequency matrices (PFMs) of the *in vivo* motifs were estimated from the height of base logos and produced using ggseqlogo (Wagih, 2017) and Logomaker (Tareen and Kinney, 2019). To eliminate the effect of sequence length on motif enrichment, we randomly selected corresponding transcript regions from length-paired co-expressed unbound genes as negative set for each transcript region of genes in the RIP-enriched gene sets (positive set). The longest transcript isoform of each gene was used. For a motif of length K and for all transcript subsequences of length K (i.e., K-mers), we calculated a "hit score" by multiplying the probability of that K-mer under the PFM and the probability of the entire subsequence being accessible at the given location within the transcript. The probability of a K-mer under a PFM was calculated by multiplying the probability of each base of the K-mer at its corresponding position in the PFM. Subsequence accessibility was estimated using RNAplfold (Bernhart et al., 2006; Lorenz et al., 2011) with the parameters: -W 80 -L 40 -u < motif_length > . For each motif, we tested its ability to distinguish positive genes from length-paired negative genes by ranking genes according to the maximum "hit score" of all subsequences of its corresponding transcript for that motif. We repeated the test 1000 times with length-paired negatives randomly selected each time, and reported the number of significant Mann-Whitney *U* tests, and the mean and standard deviation of the AUROCs and p values of each motif's significant tests (Table S3). To show the distribution of motifs in RIN targets v.s. non-targets, we grouped the number of RIN motifs (defined as sites with "hit score" >0.001) in a length-paired positive and negative sample from each of the three transcript regions into 20 bins, and used Gaussian kernels to fit the un-normalized positive and negative histogram for each region. The differences between the two corresponding Gaussian kernels in each of the three regions are displayed in Figure 2D.

Comparisons of RIN-associated mRNAs to published *Drosophila* datasets

For all comparisons of RIN-associated mRNAs to *Drosophila* transcripts reported in previously published datasets, all gene IDs from the various datasets were first updated using the FlyBase 'Upload/Convert IDs' tool to FBgn IDs from FlyBase release 6.20, to ensure consistency of identifiers between datasets. The lengths of the longest and shortest mRNA transcript isoforms for every gene were obtained from FlyBase release 6.20.

For comparisons of RIN-associated mRNAs to mRNA translation and abundance data from Eichhorn et al. (2016), only genes measured in both datasets were included in the scatterplot comparisons. In cases where a single gene had more than a single fold-enrichment value in our microarray data, due to the presence of multiple probe sets representing the same gene, the higher fold-enrichment value was used.

For comparisons of RIN-associated mRNAs to lists of genes from other datasets, including maternal decay classes, and N^6-methyladenosine (m^6A) modification, significant enrichment or depletion was assessed between the relevant lists with Fisher's exact test, using as a background the intersection of the set of expressed genes for our RIP-Chip experiment and the set of genes included in the dataset being compared, as previously described (Laver et al., 2015a).

Comparisons of RIN-associated mRNAs and proteins to datasets in other species

To compare *Drosophila* RIN-associated mRNAs and proteins to reported lists of human G3BP-associated proteins, and stress granule enriched or depleted proteins and mRNAs in yeast, mouse, and human, the *Drosophila* homologs of genes in the non-*Drosophila* datasets were obtained using the DRSC Integrative Ortholog Prediction Tool (DIOPT) web server (https://www.flyrnai.org/cgi-bin/DRSC_orthologs.pl) (Hu et al., 2011). Only *Drosophila* homologs with a 'Rank' of 'moderate' or 'high' in the DIOPT output

were considered, and where more than one *Drosophila* homolog existed, only the best match was included. After obtaining the lists of homologs, comparisons between the RIN-associated mRNAs and *Drosophila* homologs of datasets from other species were carried out as for the intra-species comparisons described above.

Gene ontology annotation enrichment analysis

GO annotation enrichment analysis was carried out using the DAVID 6.8 functional annotation tool web server (Huang et al., 2009a, 2009b), to search for enrichment of GO terms included in the GO FAT database. Genes identified by RIP-Chip as encoding RIN-associated mRNAs were analyzed for enrichment against the set of expressed genes defined for our RIP-Chip experiment, as previously described (Laver et al., 2015a). GO terms enriched at an FDR of less than 10% were considered significant.

For GO terms highlighted in scatterplots that depict transcript length and transcript translational status or abundance, lists of all genes annotated with each GO term were obtained from FlyBase using the controlled vocabulary search tool.

DATA AND CODE AVAILABILITY

The accession number for the microarray data for the RIN RIP-Chip reported in this paper is GEO: GSE12900.